An m6A-programmed cell death signature predicts prognosis and identifies STK25 as a therapeutic target in colon adenocarcinoma

HEZHI YU*, TIHUI LI*, XIAOYUN HUANG, ZIHAN CHEN, ZIXIANG LIN and FENGLIN CHEN

Department of Gastroenterology, Fujian Medical University Union Hospital, Fuzhou, Fujian 350001, P.R. China

Received November 5, 2025; Accepted March 9, 2026

DOI: 10.3892/ol.2026.15610

Abstract. Colon adenocarcinoma (COAD) remains a leading cause of cancer-related mortality worldwide. Although programmed cell death (PCD) and RNA N6-methyladenosine (m6A) modification have each been shown to regulate tumor progression and therapeutic responses, their combined prognostic significance in COAD has not been fully elucidated. The present study aimed to develop an integrated m6A-PCD prognostic model and to identify potential therapeutic targets in COAD. In total, 1,379 genes across 14 PCD-related pathways were systematically analyzed and a 21-gene m6A-PCD signature (MCDI) was constructed following multivariate Cox regression analysis. Single-cell RNA sequencing from publicly available datasets (GSE132465 and GSE205506), together with reverse transcription-quantitative PCR (qPCR) validation using clinical samples, were employed to identify genes with tumor-specific expression patterns. The functional role of serine/threonine kinase 25 (STK25) was further investigated through knockdown experiments, flow cytometry, m6A methylated RNA immunoprecipitation (MeRIP)-qPCR and RIP assays. In addition, small interfering RNAs targeting methyltransferase-like 3 (METTL3) and YTH domain-containing protein 1 (YTHDC1) were used to evaluate the involvement of m6A modification in STK25 mRNA stability and apoptosis regulation. The resulting MCDI signature demonstrated robust and independent prognostic value and effectively predicted differential responses to programmed death-ligand 1 immunotherapy. In total, 5 core genes [microRNA 210, STK25, TGFB2, tripartite motif containing (TRIM)6 and TRIM68] were identified as key prognostic markers. STK25 was specifically upregulated in tumor epithelial cells, and its knockdown significantly promoted apoptosis in COAD cells. Correlation analyses revealed positive associations between STK25 expression and multiple m6A regulators, with METTL3 and YTHDC1 showing the highest targeting credibility. Knockdown of METTL3 or YTHDC1 reduced STK25 mRNA levels. RIP assays confirmed their direct binding to STK25 mRNA, while MeRIP-qPCR demonstrated that METTL3 knockdown decreased the m6A modification level of STK25 mRNA. In conclusion, the reconstructed MCDI was established as a novel m6A-PCD-based prognostic model for patient stratification and the prediction of immunotherapy response in patients with COAD. STK25 was also identified as a potential therapeutic target linking m6A modification to the regulation of apoptosis in COAD.

Correspondence to: Dr Fenglin Chen, Department of Gastroenterology, Fujian Medical University Union Hospital, 29 Xinquan Road, Fuzhou, Fujian 350001, P.R. China
E-mail: drchenfl@fjmu.edu.cn

*Contributed equally

Key words: colon adenocarcinoma, prognostic biomarkers, N6-methyladenosine, programmed cell death, real-world study, serine/threonine kinase 25

Introduction

Colon adenocarcinoma (COAD) is a highly malignant gastrointestinal tumor characterized by difficulties in early diagnosis and an unfavorable prognosis. According to the latest global estimates, ~1.93 million new cases and >900,000 COAD-related deaths were reported in 2023, ranking COAD as the third most common cancer and the second leading cause of cancer-related mortality worldwide (1). Current therapeutic strategies, including surgical resection, chemotherapy, radiotherapy and targeted therapies (such as anti-EGFR and anti-VEGF agents), have improved outcomes for patients with early-stage disease (2). However, patients with advanced-stage COAD often derive limited survival benefit due to tumor heterogeneity, therapeutic resistance and the lack of reliable prognostic biomarkers, highlighting the urgent need for accurate risk stratification models to support individualized treatment strategies (3,4).

A previous study has underscored the critical roles of RNA epigenetic modifications, particularly N6-methyladenosine (m6A) methylation, and programmed cell death (PCD) in the pathogenesis and progression of COAD (5). m6A, the most abundant internal modification of mammalian mRNA, is dynamically regulated by 'writers' [methyltransferases such as methyltransferase-like 3 (METTL3)], 'readers' [recognition proteins such as YTH domain-containing protein 1 (YTHDC1)] and 'erasers' (demethylases), thereby influencing mRNA stability, splicing and translation (6,7). This modification plays a crucial role in regulating tumor cell behavior, including proliferation and therapeutic response (8,9). In

parallel, PCD comprises 14 regulated forms of cell death, including apoptosis, pyroptosis, ferroptosis and autophagy, which are essential for maintaining tissue homeostasis but are frequently dysregulated in cancer, facilitating tumor survival and treatment resistance (10,11). Accumulating evidence indicates that m6A modification can regulate PCD pathways by modulating the expression of key genes, thereby influencing tumor cell fate and disease progression (12,13).

Despite these advances, most previous studies have examined m6A modification and PCD in isolation, leaving a critical gap in understanding their integrated prognostic value and mechanistic interplay in COAD. In particular, the complex interaction between epitranscriptomic regulation and downstream cell death execution pathways during tumor progression has not been adequately addressed (14-17). To date and to the best of our knowledge, no comprehensive prognostic models have combined m6A regulators with PCD-related genes to predict patient outcomes or identify actionable therapeutic targets, which is essential for linking epigenetic regulation to cell death control and optimizing immunotherapy efficacy.

To address this gap, the present study aimed to systematically investigate the prognostic and biological significance of m6A modification in relation to PCD pathways in COAD. By integrating transcriptomic data from multiple cohorts, an m6A-PCD-based prognostic model was constructed to evaluate its potential for patient stratification and therapeutic response prediction. In addition, single-cell RNA sequencing datasets and clinical sample validation were used to identify tumor-specific genes associated with this signature. Functional experiments were further performed to explore the potential role of key candidate genes and to investigate the regulatory relationship between m6A modification and PCD-related molecular mechanisms in COAD.

Materials and methods

Cell line culture and transfection. Human colon cancer cell lines, RKO and LOVO, were cultured in RPMI-1640 medium (BioSharp Life Sciences) supplemented with 10% fetal bovine serum (Gibco; Thermo Fisher Scientific, Inc.) and 1% penicillin-streptomycin (Gibco; Thermo Fisher Scientific, Inc.) at 37˚C in a humidified atmosphere containing 5% CO_2. Small interfering (si)RNAs targeting METTL3, YTHDC1 and STK25 were synthesized by Shanghai GenePharma Co., Ltd. To ensure efficient gene silencing and reduce potential off-target effects, different siRNA sequences targeting the same gene were evaluated in the two cell lines, and the siRNA exhibiting the highest knockdown efficiency in each cell line was used for subsequent experiments. Transient transfections were performed using siRNA-Mate Plus transfection reagent (Shanghai GenePharma Co., Ltd.) according to the manufacturer's instructions. The siRNA premix was prepared at a concentration of 1.5 pmol/μl (~1.5 μM). Cells were transfected at 37˚C in a 5% CO_2 incubator, and transfection efficiency was assessed 48 h post-transfection. RNA extraction and subsequent RNA-based experiments were performed 48 h after transfection. The siRNA sequences used in the present study were as follows (5'-3'): RKO: siMETTL3-Homo-929 sense, GUGCAAGAAUUCUGUGACUTT; siMETTL3-Homo-929 antisense, AGUCACAGAAUUCUUGCACTT; siYTHDC1-Homo-1883 sense, GCGUCGACCAGAAGAUUAUTT; siYTHDC1-Homo-1883 antisense, GCGUCGACCAGAAGAUUAUTT; siSTK25-Homo-518 sense, GAGACAUACAUUGCCACGATT; and siSTK25-Homo-518 antisense, UCGUGGCAAUGUAUGUCUCTT. LOVO: siMETTL3-Homo-208 sense, GCACUUGGAUCUACGGAAUTT; siMETTL3-Homo-208 antisense, AUUCCGUAGAUCCAAGUGCTT; siYTHDC1-Homo-1595 sense, GCUGGGAGGUGUCUUUAAATT; siYTHDC1-Homo-1595 antisense, UUUAAAGACACCUCCCAGCTT; siSTK25-Homo-288 sense, GCAUCGAUAACCACACAAATT; and siSTK25-Homo-288 antisense, UUUGUGUGGUUAUCGAUGCTT.

Patient tissue samples. Colon cancer tissues and matched adjacent normal tissues were collected from 10 patients who underwent radical surgical resection at Fujian Medical University Union Hospital (Fuzhou, China) between December 1, 2025, and December 31, 2025. Adjacent normal tissues were obtained from areas located at least 5 cm away from the tumor margin. The cohort included 5 male and 5 female patients, with a median age of 55.5 years (range, 35-74 years). The inclusion criterion was histologically confirmed colon adenocarcinoma in patients who had not received preoperative chemotherapy or radiotherapy. Patients who had received neoadjuvant therapy or had incomplete clinical information were excluded. Written informed consent was obtained from all participants, and the study was approved by the Institutional Ethics Committee of Fujian Medical University Union Hospital (approval no. 2025KY307).

Cell apoptosis assay. Cell apoptosis was assessed by flow cytometry using an Annexin V-FITC/PI Apoptosis Detection Kit (Beyotime Biotechnology). Briefly, cells were resuspended in binding buffer, incubated with Annexin V-FITC and PI in the dark for 30 min at room temperature. Samples were analyzed using a BD FACSCanto II flow cytometer (BD Biosciences), and data were processed using FlowJo software (version 10.8.1; BD Biosciences).

Western blotting. Cell pellets derived from paired tumor and adjacent normal tissues were lysed in RIPA buffer (cat. no. P0013B; Beyotime Biotechnology), and protein concentrations were determined using a BCA Protein Assay Kit. Equal amounts of protein (40 μg) were separated on 10% gels using SDS-PAGE and transferred onto PVDF membranes. Membranes were blocked with 5% non-fat milk for 2 h at room temperature and then incubated overnight at 4˚C with the primary STK25 polyclonal antibody (cat. no. 25821-1-AP, 1:1,000 dilution; Proteintech Group, Inc.). The membranes were also incubated with GAPDH antibody (cat. no. 60004-1-Ig; 1:5,000 dilution; Proteintech Group, Inc.) as a loading control. After three washes with TBST (TBS containing 0.05% Tween-20; 5 min each), membranes were incubated with horseradish peroxidase-conjugated secondary antibodies (cat. no. A0208; 1:5,000 dilution; Beyotime Biotechnology) for 1 h at room temperature. Membranes were washed again as aforementioned and protein bands were detected using an enhanced chemiluminescence detection kit (cat. no. P0018; Beyotime Biotechnology), with reagents A and B mixed at

a 1:1 ratio in the dark. The chemiluminescent signals were captured using a ChemiDoc XRS+ imaging system (Bio-Rad Laboratories, Inc.).

Reverse transcription-quantitative PCR (RT-qPCR). Total RNA from the cells was extracted using QIAzol reagent (Qiagen, Inc.). Subsequently, 2 μg of total RNA was reverse-transcribed into cDNA using a commercial reverse transcription kit (PrimeScript™ RT Reagent Kit; cat. no. RR047A; Takara Bio, Inc.) according to the manufacturer's instruction. PCR amplification was performed using SYBR GREEN qPCR Master Mix TB Green® Premix Ex Taq™ II; cat. no. RR820A; Takara Bio, Inc.) on an ABI 7500 Real-Time PCR System (Applied Biosystems; Thermo Fisher Scientific, Inc.). The thermocycling conditions were as follows: Initial denaturation at 95˚C for 30 sec, followed by 40 cycles of 95˚C for 5 sec and 60˚C for 34 sec. GAPDH was used as an internal control. Relative gene expression levels were calculated using the $2^{-\Delta\Delta Cq}$ method (18). The primer sequences used were as follows (5'-3'): STK25 forward, GCACAGCAAGCCCTTCAAGG; STK25 reverse, CGTCCCCTTGTGAAGCTTGC; METTL3 forward, CTACGGAATCCAGAGGCAGCATTG; METTL3 reverse, GAGATGGCAAGACAGATGGACACAG; YTHDC1 forward, TGGAGAGGAGGAGGAGGAAGAGG; YTHDC1 reverse, CGGACAGCACGAACGGAAGATG; GAPDH forward, CAAGGCTGTGGGCAAGGTCATC; and GAPDH reverse, GTGTCGCTGTTGAAGTCAGAGGAG.

RNA immunoprecipitation (RIP) assay. RIP assays were performed using a RIP Kit (cat. no. 17-700; Merck KGaA) according to the manufacturer's instructions. Briefly, magnetic beads were incubated overnight at 4˚C with 5 μg of antibodies against METTL3 (Cohesion Biosciences Limited; cat. no. CQA1783) or YTHDC1 (Abcam; cat. no. ab264375) or normal IgG as a negative control (Beyotime Biotechnology, cat. no. A7016). The antibody-conjugated beads were then incubated with 500 μg of cell lysates, followed by washing five times using the RIP washing buffer provided in the kit. RNA-protein complexes were digested with proteinase K at 55˚C for 30 min, and the bound RNA was subsequently eluted using the RIP elution buffer supplied with the kit, purified and analyzed by RT-qPCR to determine enrichment levels. The enrichment of target transcripts (STK25 mRNA) was assessed. The aforementioned primers used in the RT-qPCR were used for the analysis.

m6A methylated RIP-qPCR (MeRIP-qPCR). MeRIP was performed using the MeRIP m6A Kit (cat. no. GS-ET-001A; Cloud-Seq Biotech Ltd. Co.) following the manufacturer's protocol. Briefly, 5 μg of chemically fragmented RNA was immunoprecipitated using 5 μg of anti-m6A antibody. The precipitated RNA and input RNA (control) were then analyzed by RT-qPCR using specific primers for STK25 (5'-3'): Forward, TTCTGAAGGGCCTGGATTATCTGC and reverse, TTCTTGGGAATCAGGAACAGGACGC.

Gene set sources and The Cancer Genome Atlas (TCGA) data processing. Gene sets associated with different forms of PCD were curated from published literature (19,20) and databases (FerrDb, www.zhounan.org/ferrdb; HADb, http://autophagy.lu/clustering/index.html). For each PCD type, a corresponding gene list was compiled based on these sources. The number in parentheses indicates the number of genes included in each gene set. Specifically, the curated gene sets included: Apoptosis (n=580), autophagy (n=525), lysosome-dependent cell death (n=220), necroptosis (n=105), ferroptosis (n=104), pyroptosis (n=64), immunogenic cell death (n=40), cuproptosis (n=21), entotic cell death (n=19), NETotic cell death (n=10), alkaliptosis (n=8), parthanatos (n=7), oxeiptosis (n=5) and disulfidptosis (n=4). The gene expression dataset for COAD was obtained from TCGA database (https://www.cancer.gov/ccg/research/genome-sequencing/tcga). Data preprocessing was conducted using the R package (version 4.5.0), TCGAbiolinks (version 2.30.1). Raw expression matrices were subjected to quality control (QC) with the TCGAanalyze_Preprocessing function (cor.cut=0.6) to remove low-quality samples. Technical biases were corrected using the TCGAanalyze_Normalization function and low-expression genes were filtered out with the TCGAanalyze_Filtering function (qnt.cut=0.25). Differential expression analysis between tumor and adjacent normal tissues was performed using the edge R package (version 3.42.4). Genes with $P<0.05$ were considered significantly differentially expressed genes (DEGs). PCD-related DEGs were identified by intersecting the DEG list with predefined PCD-related gene sets. Gene Ontology (GO) and Kyoto Encyclopedia of Genes and Genomes (KEGG) pathway enrichment analyses of upregulated and downregulated DEGs were conducted separately using the enrichGO and enrichKEGG functions from the clusterProfiler (version 4.8.1).

Construction of the MCDI clinical prediction model. Univariate Cox regression analysis of PCD-related genes was performed using the survival (version 3.5-5) R package. Spearman correlation analysis between PCD-related genes and m6A regulators was conducted using the Hmisc package (version 5.1-1). Genes that were significant in the univariate analysis and correlated with m6A regulators were combined and LASSO Cox regression was applied using the glmnet package (version 4.1-8) to select the final signature genes. The risk score for each patient, designated the MCDI, was calculated using the following formula: MCDI = (0.011510365 x ATG13 exp.) + (-0.013042804 x CARS1 exp.) + (-0.020456124 x DEF8 exp.) + (0.016717586 x FBH1 exp.) + (0.020419640 x FLCN exp.) + (0.016380593 x IDUA exp.) + (-0.031405568 x ING5 exp.) + (0.048748645 x MIR210 exp.) + (0.025716205 x PIDD1 exp.) + (0.009329190 x PIP4K2B exp.) + (-0.015689712 x PLA2G15 exp.) + (0.033027922 x STK25 exp.) + (0.099700295 x TGFB2 exp.) + (0.015789901 x TRADD exp.) + (0.001302880 x TRAF2 exp.) + (0.346873020 x TRIM6 exp.) + (0.068723205 x TRIM68 exp.) + (0.006337617 x TYK2 exp.) + (-0.014371960 x USP21 exp.) + (-0.012858944 x WDR6 exp.) + (0.003176967 x ZFYVE1 exp.). Within these formulae, 'exp.' designates the normalized expression level of each gene in the TCGA dataset.

Construction of the similarity network for the 21 PCD-related genes. A co-expression network among the 21 signature genes was constructed based on Spearman correlation analysis ($|R|>0.15$, $P<0.05$) and visualized using Cytoscape software (version 3.10.1; Cytoscape Consortium).

Differential expression analysis between high- and low-risk groups in TCGA-COAD dataset. Differential expression analysis between the MCDI-defined high- and low-risk groups in the TCGA-COAD cohort was conducted using the edge R package (version 3.42.4). Patients were stratified into high- and low-risk groups according to the optimal cutoff value of the MCDI score determined by the surv_cutpoint function in the survminer (version 0.4.9) R package. Gene expression data were first normalized using the Trimmed Mean of M-values method. Genes with a false discovery rate (FDR) <0.05 and an absolute log2 fold change (|log2FC|)>1 were considered statistically significant DEGs. The resulting DEG list was subsequently used for functional enrichment analyses.

Independent prognostic value of MCDI. Clinical data from the TCGA-COAD cohort and external validation cohorts (GSE39582, GSE33113, GSE38832, GSE67501, GSE78220) (21-25), including age, sex, overall tumor stage (Stages I-IV) and T, N and M stages of the TNM system, were collected. Univariate and multivariate Cox regression analyses were performed, incorporating these clinical variables alongside the MCDI score, to assess the independent prognostic value of the MCDI in predicting patient survival. Additionally, a prognostic nomogram was constructed using multivariate Cox regression combined with stepwise regression, integrating the MCDI score and clinical characteristics (age, sex, overall stage, T stage and N stage). The nomogram was visualized using the regplot (version 1.1) R package.

Correlation analysis between MCDI and immune checkpoint gene expression. The association between the MCDI score and the expression levels of immunomodulatory genes was assessed by calculating Spearman correlation coefficients using the rcorr function from the R Hmisc package.

Tumor immune microenvironment analysis. The relative proportions of 22 immune cell types in each TCGA-COAD sample were estimated using the CIBERSORT tool (https://github.com/Moonerss/CIBERSORT). The Tumor Immune Dysfunction and Exclusion (TIDE) score for each sample was calculated via the online TIDE tool (http://tide.dfci.harvard.edu/) to predict potential responses to immune checkpoint blockade (ICB) therapy. Somatic mutation data (simple nucleotide variation) for the TCGA-COAD cohort were obtained from the Genomic Data Commons portal (https://portal.gdc.cancer.gov) using the TCGAbiolinks R package. Tumor mutational burden (TMB) was calculated with the maftools package (version 2.8.05), normalizing by an exonic capture region size of 38 Mb, and the resulting values were log-transformed. Microsatellite instability (MSI) status data were retrieved from the TCGA-COAD phenotype dataset available through the UCSC Xena database (https://xenabrowser.net/datapages/).

Single-cell RNA sequencing (scRNA-seq) data analysis. In total, 2 colon cancer-related scRNA-seq datasets (GSE132465 and GSE205506) were used for analysis (26,27). Data processing and analysis were conducted using the Seurat R package (v4.4.0). QC was applied to remove low-quality cells. After QC, data were normalized and integrated to correct for batch effects using the reciprocal principal component analysis (RPCA) method. Cells were clustered and annotated into six major cell types based on canonical marker genes. Epithelial cells were then extracted and divided into tumor and control groups according to the sample type. These epithelial cells were subjected to unsupervised re-clustering to identify distinct subpopulations. The copy number variation (CNV) profile of each epithelial subcluster was assessed using the inferCNV (version 1.18.1) R package to evaluate malignant potential. Malignant epithelial subpopulations were identified based on CNV inference for downstream analyses. Expression patterns of the gene of interest (STK25) and a known colorectal cancer malignant epithelial marker (carcinoembryonic antigen-related cell adhesion molecule 6; CEACAM6) were examined within these malignant cells. Differential expression analysis between tumor and control groups was performed using the FindMarkers function. The MCDI score was then calculated for each single cell and its distribution was visualized across different cell types, sample groups and epithelial subpopulations.

Correlation analysis of STK25 with COAD. The association between STK25 expression and clinical parameters (MCDI, T stage, N stage, M stage and age) in the TCGA-COAD cohort was assessed. Kaplan-Meier survival curves were generated using the ggsurvplot function from the survminer (version 0.4.9) R package to visualize the impact of STK25 expression levels on patient overall survival (OS).

Prediction of upstream m6A regulators for STK25. To investigate the expression correlation between STK25 and 23 known m6A regulatory enzymes, Spearman rank correlation analysis was performed to calculate correlation coefficients (ρ) and corresponding P-values. Results were visualized using the ggplot2 (version 3.5.1) R package.

The RM2Target database (http://rm2target.canceromics.org/), which provides information on potential associations between m6A regulators and their target genes, was subsequently utilized. STK25 was input as the target gene to search for potential m6A regulatory enzymes modulating its expression. During screening, a confidence score threshold >4 was applied to ensure high reliability of the results. Based on this criterion, two potential m6A regulators were identified: YTHDC1 and METTL3.

Protein-protein interaction (PPI) network construction. To explore potential functional interactions among the signature genes, a protein-protein interaction (PPI) network was constructed using the STRING database (version 12.0; https://string-db.org/). The list of the 21 signature genes was uploaded to STRING, and interactions with a minimum required interaction score >0.4 (medium confidence) were retained. The resulting interaction network was then imported into Cytoscape (version 3.10.1; https://cytoscape.org/) for visualization and network analysis.

Statistical analysis. Statistical analyses were conducted using R software (version 4.3.2) and GraphPad Prism (version 9; Dotmatics). Data are presented as the

mean ± standard deviation. Comparisons between two groups were performed using both paired and unpaired two-tailed Student's t-test. For comparisons among multiple groups, one-way analysis of variance (ANOVA) followed by the Tukey post hoc test was applied. When the data did not follow a normal distribution, the Wilcoxon rank-sum test was used. The χ^2 test was applied for categorical variables. Spearman correlation analysis was performed to evaluate associations between continuous variables. Two-sided P<0.05 was considered to indicate a statistically significant difference. Multivariate Cox proportional hazards regression analysis was performed on the 21 PCD-related genes using the coxph function in the R survival package to assess whether their expression levels were independent prognostic factors.

Results

Dysregulation of PCD Genes in COAD. To characterize the landscape of PCD in COAD, the TCGA-COAD transcriptomic dataset was analyzed, focusing on 1,379 genes representing 14 distinct PCD modalities curated from the literature and databases (Fig. 1A). Differential expression analysis revealed widespread dysregulation of PCD-related genes in tumor tissues compared with adjacent normal tissues, with 438 genes significantly upregulated and 393 downregulated (Fig. 1B).

GO enrichment analysis showed that upregulated PCD genes were primarily involved in apoptosis- and autophagy-related processes, including 'regulation of apoptotic signaling pathway', 'intrinsic apoptotic signaling pathway' and 'regulation of autophagy'. Downregulated genes were enriched in pathways associated with 'regulation of autophagy', 'lysosomal organization' and 'myeloid leukocyte mediated immunity', indicating that multiple PCD-related processes are transcriptionally altered in COAD rather than uniformly activated or suppressed (Fig. 1C).

KEGG analysis revealed similar patterns: 'Lysosome' and 'Necroptosis' pathways were enriched among the upregulated genes, whereas 'autophagy - animal', 'Lysosome', 'Apoptosis' and 'Necroptosis' pathways were enriched among downregulated genes (Fig. 1D). The recurrence of apoptosis-, autophagy- and lysosome-related terms in both upregulated and downregulated gene sets suggests broad remodeling of these pathways in COAD, involving simultaneous activation and inhibition of distinct gene subsets within the same cell death networks.

Overall, these results indicate that PCD-related pathways undergo complex transcriptional alterations in COAD, providing a molecular foundation for subsequent integrative analysis of m6A modification and PCD.

Integration of m6A regulation and PCD genes in COAD. To develop an integrated m6A-PCD prognostic model, a systematic analysis of 1,379 genes across 14 PCD pathways was first conducted from the TCGA-COAD cohort. Univariate Cox regression identified 109 PCD-related genes significantly associated with OS (P<0.05; Fig. 2A). Concurrently, Spearman correlation analysis showed that 957 PCD genes were significantly co-expressed with multiple m6A regulators (|R|>0.2, P<0.05; Fig. 2B), indicating extensive transcriptional interplay between m6A modification and PCD in COAD. By integrating differential expression, survival association and m6A correlation analyses, 31 overlapping hub genes that were dysregulated, prognostically relevant and co-expressed with m6A regulators were identified (Fig. 2C). Subsequent LASSO Cox regression refined this panel to a 21-gene core signature, constituting the MCDI (Fig. 2D), of which 15 genes were upregulated and 6 were downregulated in COAD tumors (Fig. 2E).

To investigate functional relationships, a protein-protein interaction network was constructed, revealing a central cluster of highly connected hub proteins including FBH1, STK25, TYK2, DEF8, PLA2G15, PIP4K2B, ATG13, ING5, WDR6 and USP21 surrounded by peripheral nodes (Fig. 2F). These core genes may serve as key integrators linking m6A modification with PCD regulation, potentially underlying the heterogeneous cell-death dynamics and immune responses observed in COAD.

Development and validation of the MCDI prognostic signature for COAD. Using the 21 key m6A-regulated PCD genes identified above, a prognostic model for COAD, termed the MCDI, was constructed. Patients in both the internal validation cohort (TCGA-COAD) and external validation cohorts (GSE39582, GSE33113 and GSE38832) were stratified into high- and low-risk groups based on the median MCDI score. Each patient received a composite MCDI score calculated from the expression levels of the 21 genes, with higher scores indicating a higher predicted mortality risk. Kaplan-Meier analysis demonstrated that patients in the high-risk group had a significantly shorter OS time than those in the low-risk group in both the internal (TCGA-COAD) and external validation cohorts (all log-rank P<0.001), confirming the robust and reproducible prognostic performance of the model (Fig. 3A and B). Time-dependent ROC curve analysis was performed to evaluate the predictive performance of the MCDI model. The area under the ROC curve (AUC) was calculated to assess prognostic accuracy. In the training cohort, the AUC values for predicting 1- and 3-year overall survival were 0.609 and 0.572, respectively. In the testing cohort, the AUC values increased to 0.783 and 0.711, respectively. Similar predictive performance was observed in the validation cohorts, with AUC values of 0.805 and 0.699, and 0.584 and 0.635 for 1- and 3-year survival (Fig. 3C), indicating a moderate but stable prognostic performance of the MCDI model across different cohorts.

To explore the biological basis of MCDI-based risk stratification, a comprehensive transcriptomic comparison between the high- and low-risk groups in the TCGA-COAD cohort was performed. Differential expression analysis using the edge R package, with thresholds of FDR <0.05 and |log2FC|>1, identified 2,520 significantly dysregulated genes, including 802 upregulated and 1,718 downregulated genes in high-risk patients compared with low-risk patients (Fig. 4A).

Functional enrichment analysis of these DEGs was subsequently performed to elucidate their biological significance. GO and KEGG pathway analyses consistently indicated that the DEGs were highly enriched in processes related to apoptosis, autophagy, lysosomal function and immune regulation (Fig. 4B-D). Further association analyses with clinical characteristics showed that the MCDI score increased progressively with tumor advancement. Patients with advanced-stage clinicopathological features tended to exhibit higher MCDI

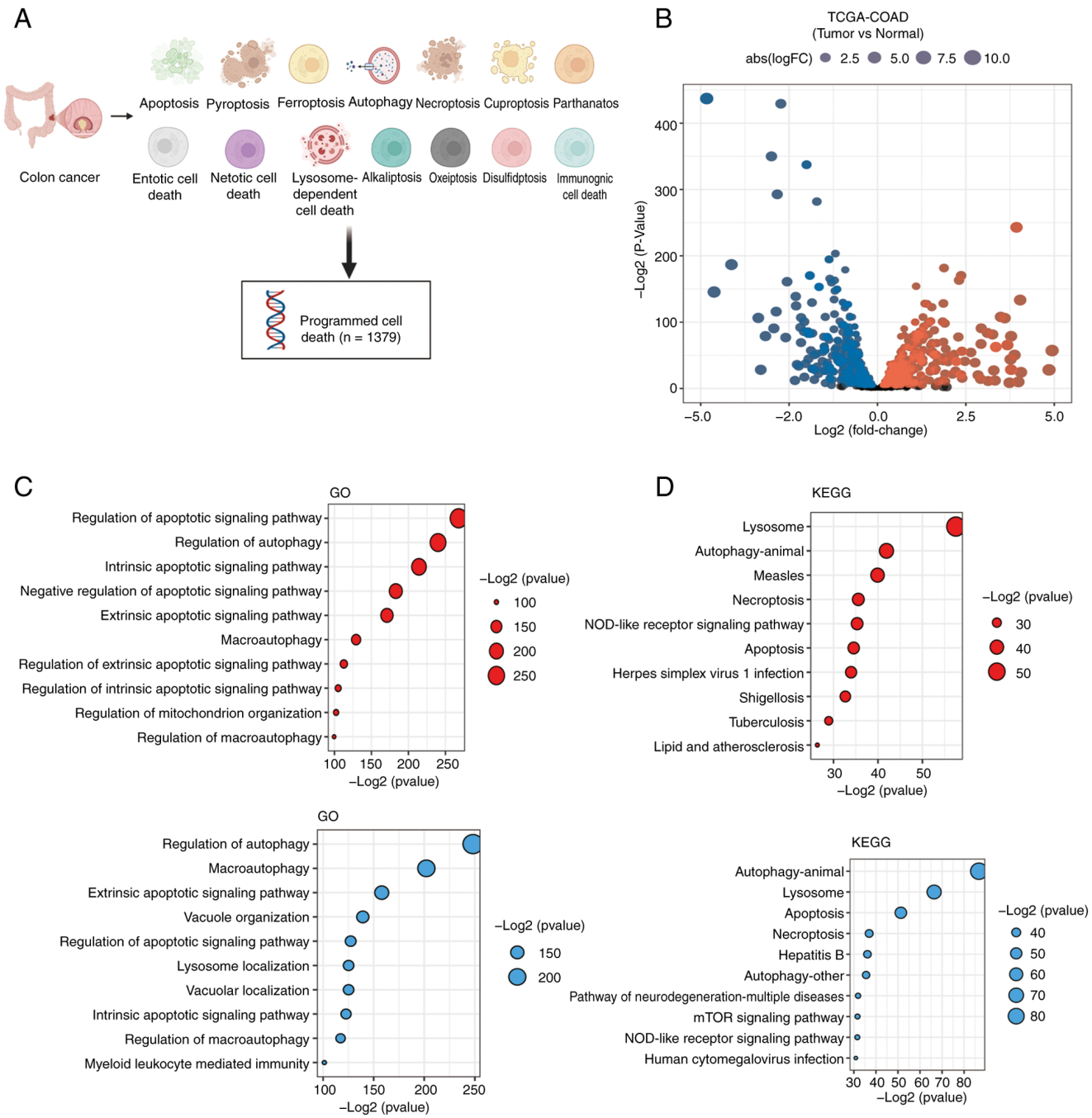

Figure 1. Transcriptomic landscape of programmed cell death-related genes in COAD. (A) The set of 1,379 genes covering the 14 programmed cell death pathways analyzed in the present study. (B) Volcano plot illustrating differentially expressed genes between tumor and normal tissues in the TCGA-COAD cohort. Gray dots indicate genes without significant differential expression (P≥0.05), whereas red and blue dots denote genes significantly upregulated and downregulated in tumor tissues, respectively (P<0.05). Bubble plots showing (C) GO and (D) KEGG enrichment analyses of the differentially expressed genes. Bubble size reflects enrichment significance [-$\log_2$(P-value)], and color indicates the direction of regulation (red, upregulated gene sets; blue, downregulated gene sets). COAD, colon adenocarcinoma; TCGA, The Cancer Genome Atlas; abs, absolute value; FC, fold-change; GO, Gene Ontology; KEGG, Kyoto Encyclopedia of Genes and Genomes.

scores. Stage IV tumors showed significantly higher MCDI scores compared with Stage I and Stage II tumors, whereas differences between other stage groups were not statistically significant (Fig. 4E). For T stage, a significant difference was observed only between T2 and T3 tumors, while other comparisons were not significant. Regarding lymph node status, patients with N1 or N2 disease exhibited significantly higher MCDI scores than those with N0, although no significant difference was observed between N1 and N2 groups. In addition, patients with distant metastasis (M1) showed significantly higher MCDI scores than those without metastasis (M0). MCDI scores were also modestly higher in patients aged >55 years and were significantly elevated in deceased patients compared with those alive (Fig. 4E). Although differences across early-stage and age subgroups were relatively modest, patients who died exhibited significantly higher MCDI scores than those who remained alive, suggesting that elevated MCDI is associated with poorer survival outcomes.

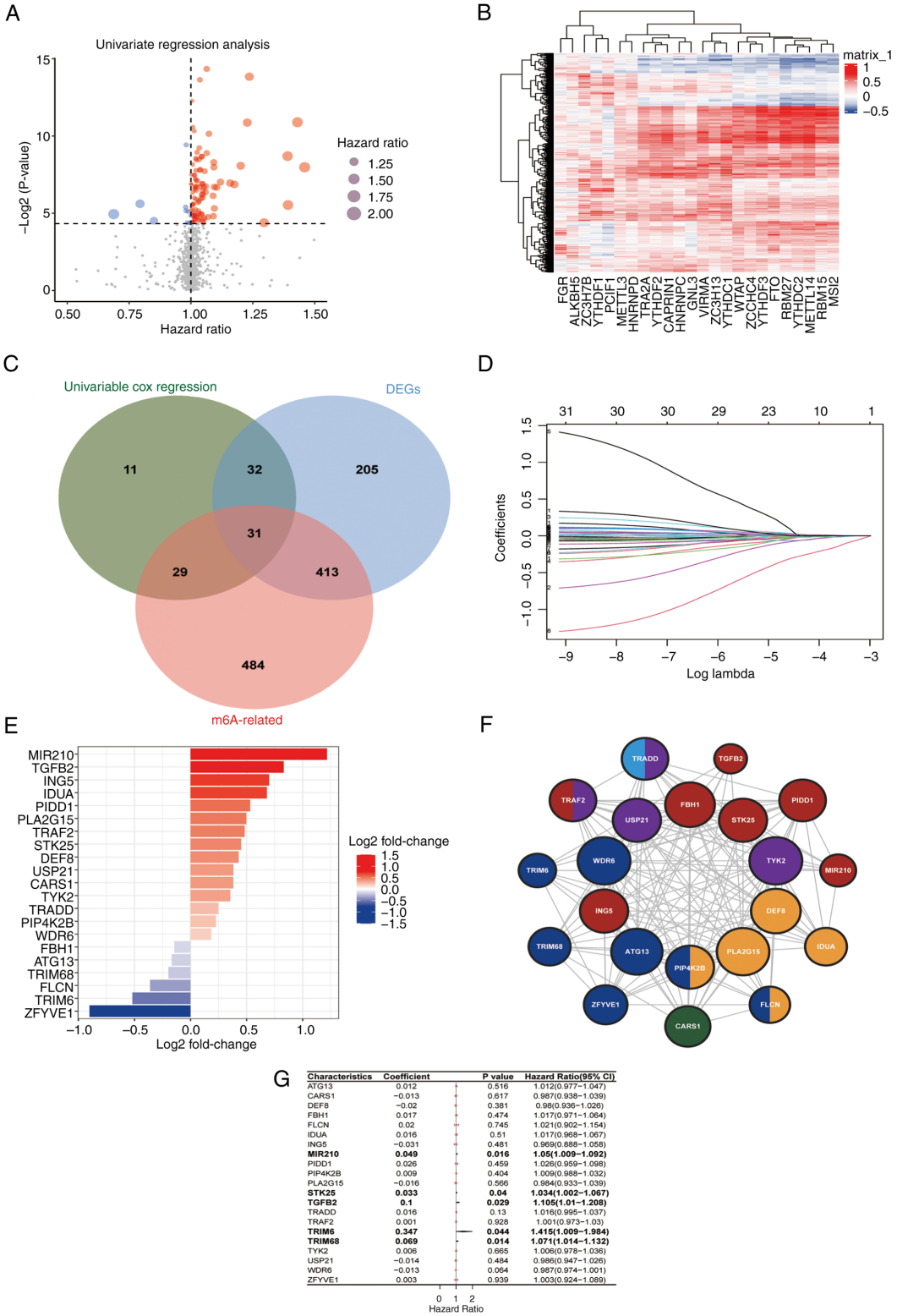

Characteristics	Coefficient	P value	Hazard Ratio(95% CI)
ATG13	0.012	0.516	1.012(0.977−1.047)
CARS1	−0.013	0.617	0.987(0.938−1.039)
DEF8	−0.02	0.381	0.98(0.936−1.026)
FBH1	0.017	0.474	1.017(0.971−1.064)
FLCN	0.02	0.745	1.021(0.902−1.154)
IDUA	0.016	0.51	1.017(0.968−1.067)
ING5	−0.031	0.481	0.969(0.888−1.058)
MIR210	**0.049**	**0.016**	**1.05(1.009−1.092)**
PIDD1	0.026	0.459	1.026(0.959−1.098)
PIP4K2B	0.009	0.404	1.009(0.988−1.032)
PLA2G15	−0.016	0.566	0.984(0.933−1.039)
STK25	**0.033**	**0.04**	**1.034(1.002−1.067)**
TGFB2	**0.1**	**0.029**	**1.105(1.01−1.208)**
TRADD	0.016	0.13	1.016(0.995−1.037)
TRAF2	0.001	0.928	1.001(0.973−1.03)
TRIM6	**0.347**	**0.044**	**1.415(1.009−1.984)**
TRIM68	**0.069**	**0.014**	**1.071(1.014−1.132)**
TYK2	0.006	0.665	1.006(0.978−1.036)
USP21	−0.014	0.484	0.986(0.947−1.026)
WDR6	−0.013	0.064	0.987(0.974−1.001)
ZFYVE1	0.003	0.939	1.003(0.924−1.089)

Figure 2. Construction of the MCDI. (A) Volcano plot of the univariate Cox regression analysis for PCD-related genes. Dot size corresponds to the HR value; red dots denote risk factors (HR>1), blue dots indicate protective factors (HR<1) and gray dots represent genes with P≥0.05. (B) Heatmap illustrating Spearman correlations between differentially expressed PCD-related genes and 23 m6A regulators in the TCGA-COAD cohort. The color gradient reflects the correlation coefficients. (C) Venn diagram showing the overlap among the prognostic genes identified by univariate Cox regression, tumor-normal differentially expressed genes and genes associated with m6A regulators, yielding 31 hub genes. (D) Coefficient profiles from the LASSO-Cox regression, showing the trajectories of model coefficients as log(λ) increases. The vertical dashed line indicates the optimal λ value determined by the minimum criterion, corresponding to 21 genes with non-zero coefficients. (E) Box plots depicting the expression levels of the 21 genes comprising the MCDI signature in tumor versus adjacent normal tissues in the TCGA-COAD cohort. (F) Protein-protein interaction network of the 21 PCD-related genes. Nodes represent genes, edges indicate significant co-expression relationships and node colors denote the primary cell death modality associated with each gene. (G) Forest plot from multivariate Cox regression analysis of the 21 genes, identifying MIR210, STK25, TGFB2, TRIM6 and TRIM68 as independent prognostic factors. MCDI, m6A-PCD integrated signature; HR, hazard ratio; PCD, programmed cell death; TCGA, The Cancer Genome Atlas; COAD, colon adenocarcinoma; MIR210, microRNA-210; STK25, serine/threonine kinase 25; TGFB2, transforming growth factor β2; TRIM6, tripartite motif containing 6; TRIM68, tripartite motif containing 68; DEGs, differentially expressed genes.

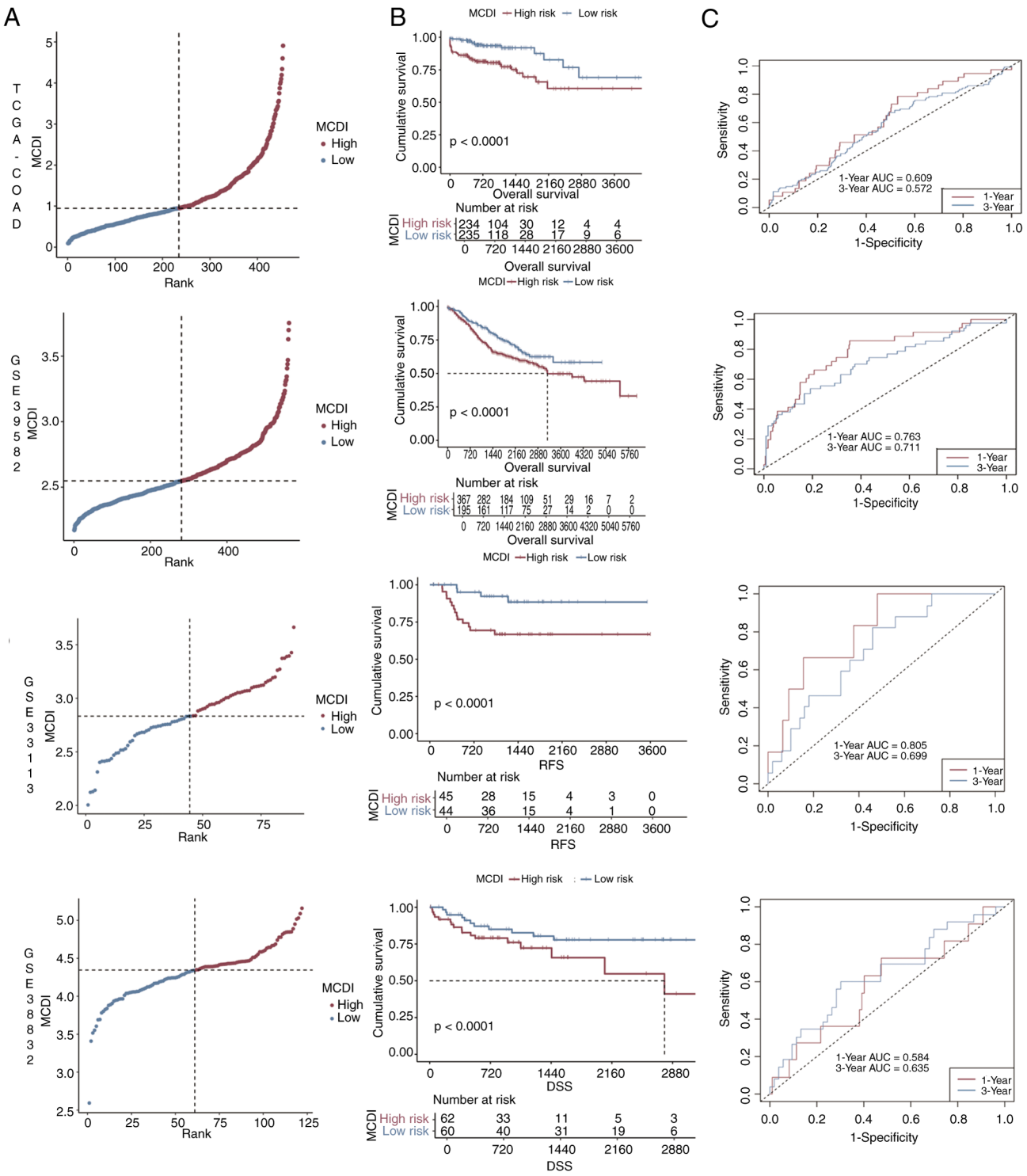

Figure 3. Validation of the MCDI. (A) Distribution of MCDI scores, corresponding risk group assignment, and survival status of patients in the TCGA-COAD, GSE39582, GSE33113 and GSE38832 cohorts. (B) Kaplan-Meier overall survival curves comparing high- and low-risk groups stratified by the median MCDI score in the TCGA-COAD, GSE39582, GSE33113 and GSE38832 cohorts. (C) Time-dependent receiver operating characteristic curves evaluating the performance of the MCDI model in predicting 1- and 3-year overall survival in the TCGA-COAD, GSE39582, GSE33113 and GSE38832 cohorts. MCDI, m6A-PCD integrated signature; PCD, programmed cell death; TCGA, The Cancer Genome Atlas; COAD, colon adenocarcinoma; AUC, area under the curve.

To determine whether the MCDI serves as an independent prognostic indicator beyond conventional clinical parameters, clinicopathologic data from the TCGA-COAD cohort were analyzed. Cox regression analyses confirmed the independent prognostic value of the MCDI. In univariate analysis, tumor stage, age, T, N and M stages and MCDI were all significant predictors of OS (Fig. 5A). All clinically relevant variables, including sex, were simultaneously entered into the multivariate Cox model. Although sex did not reach statistical significance in univariate analysis, it was included as a pre-specified covariate based on its clinical relevance, to control for potential confounding on the primary variables of

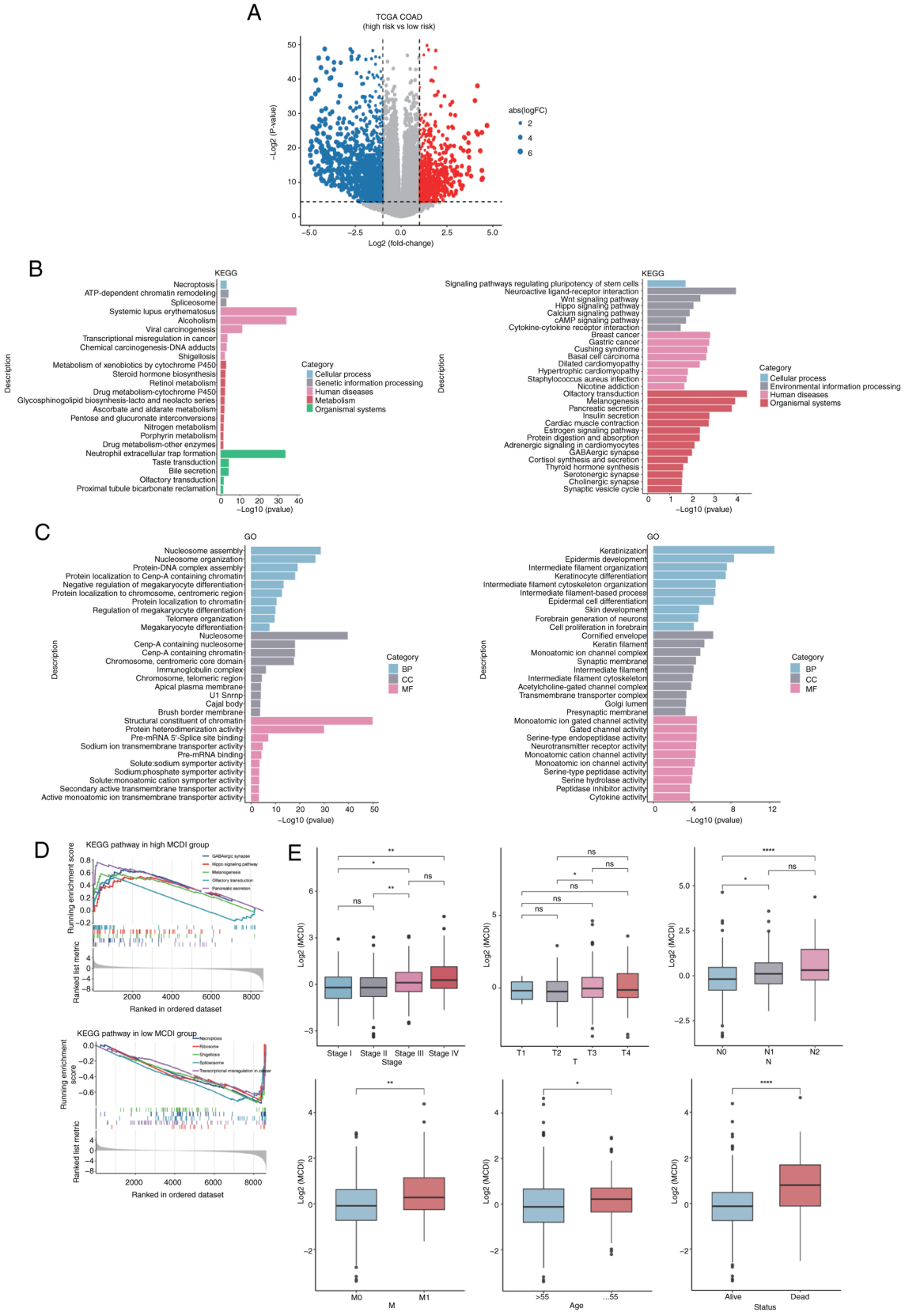

Figure 4. Biological characteristics and clinical associations of MCDI-based risk stratification. (A) Volcano plot showing differentially expressed genes between the MCDI-defined high- and low-risk groups in the TCGA-COAD cohort. Gray dots indicate genes without significant differences, whereas red and blue dots denote genes significantly upregulated and downregulated in the high-risk group, respectively (false discovery rate <0.05 and $|\log_2 FC|>1$). (B) KEGG pathway enrichment analysis and (C) GO functional enrichment analysis of differentially expressed genes between the high- and low-MCDI risk groups. (D) Gene Set Enrichment Analysis illustrating representative pathways differentially enriched between the high- and low-MCDI groups. (E) Box plots depicting the distribution of MCDI scores across clinicopathological subgroups, including overall tumor stage, T stage, N stage, M stage, age and survival status. *P<0.05, **P<0.01, ****P<0.0001. ns, not significant; MCDI, m6A-PCD integrated signature; PCD, programmed cell death; TCGA, The Cancer Genome Atlas; COAD, colon adenocarcinoma; FC, fold-change; KEGG, Kyoto Encyclopedia of Genes and Genomes; GO, Gene Ontology; BP, biological process; CC, cellular component; MF, molecular function.

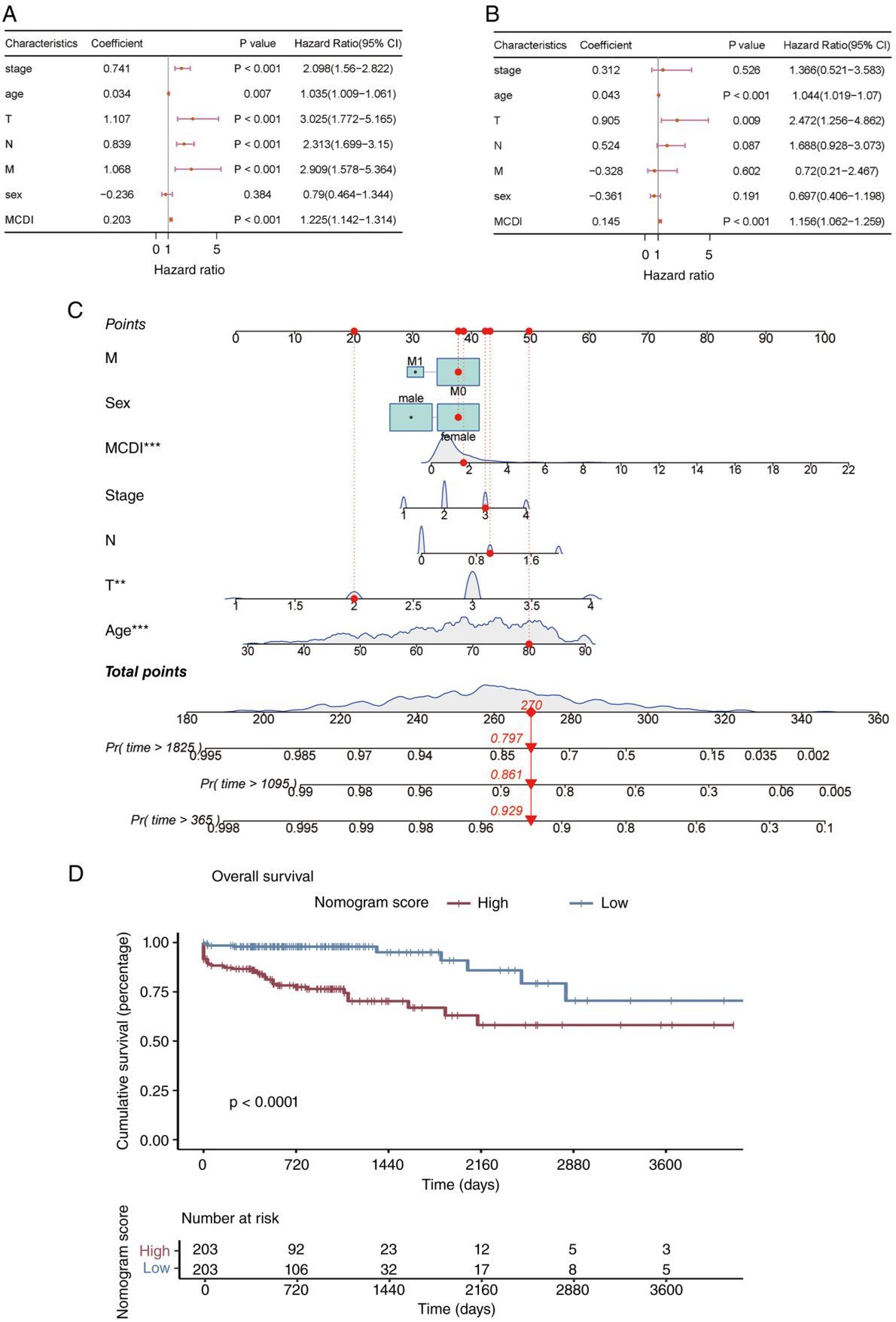

Figure 5. Independent prognostic value of the MCDI and nomogram construction. Forest plots showing the results of the (A) univariate and (B) multivariate Cox proportional hazards regression analyses assessing the effects of the MCDI score and clinicopathological variables on overall survival. (C) Prognostic nomogram integrating the MCDI score, age and T stage to estimate the 1- and 3-year overall survival probabilities in patients with colon adenocarcinoma. (D) Kaplan-Meier overall survival curves for the high- and low-risk groups stratified by the total nomogram score (using the optimal cut-off point determined by the surv_cutpoint function). **P<0.01, ***P<0.001. MCDI, m6A-PCD integrated signature; PCD, programmed cell death.

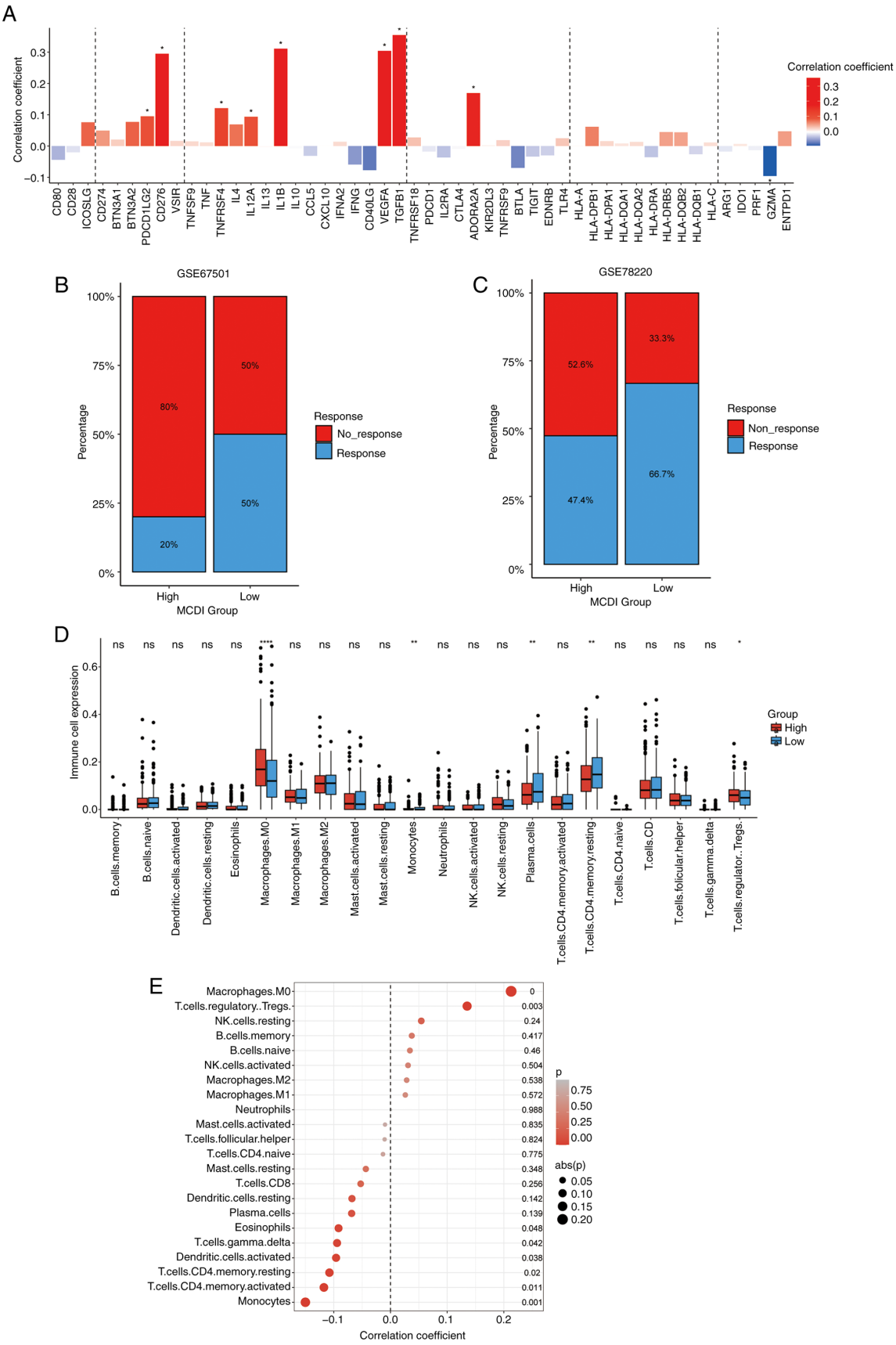

Figure 6. Association of the MCDI score with the immune microenvironment and immunotherapy response. (A) Bar plot illustrating Spearman correlations between the MCDI score and the expression levels of immunomodulatory molecules. Bar height and color intensity reflect the correlation coefficients. Comparison of the response rates to anti-PD-L1 therapy between the high- and low-MCDI groups in independent immunotherapy cohorts: (B) GSE67501 (renal cell carcinoma) and (C) GSE78220 (melanoma). (D) Box plots comparing the relative infiltration of 22 immune cell types between high- and low-MCD.I groups in the TCGA-COAD cohort. (E) Bar plot showing Spearman correlation analyses between the MCDI score and the infiltration levels of different immune cell types. *P<0.05, **P<0.01, ****P<0.0001. ns, not significant. MCDI, m6A-PCD integrated signature; PCD, programmed cell death; TCGA, The Cancer Genome Atlas; COAD, colon adenocarcinoma.

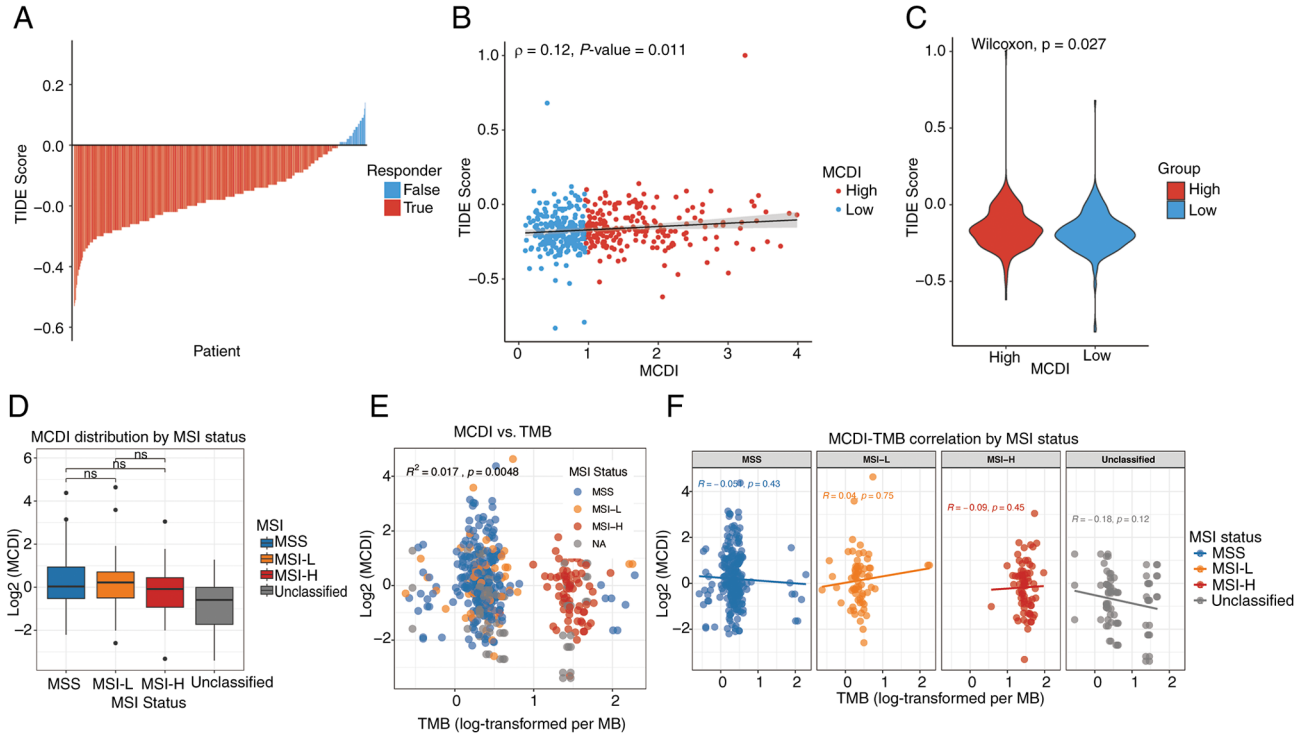

Figure 7. Association of MCDI score with immune evasion potential and genomic biomarkers. (A) Distribution of TIDE scores between responders and non-responders to immune checkpoint inhibitors in the TCGA-COAD cohort. (B) Scatter plot showing the Spearman correlation between the MCDI score and the TIDE score. (C) Violin plot comparing TIDE scores between the high- and low-MCDI groups. (D) Distribution of MCDI scores across MSI subtypes. Box plots show no significant differences among MSS, MSI-L, MSI-H and unclassified groups. (E) Correlation between MCDI and TMB. The scatter plot shows a weak but statistically significant positive correlation. (F) MSI subtype-stratified correlation analysis: Scatter plots showing MCDI-TMB correlations within each MSI subtype. ns, not significant; MCDI, m6A-PCD integrated signature; TIDE, Tumor Immune Dysfunction and Exclusion; PCD, programmed cell death; TCGA, The Cancer Genome Atlas; COAD, colon adenocarcinoma; MSS, microsatellite stable; MSI-L, microsatellite instability-low; MSI-H, microsatellite instability-high; TMB, tumor mutational burden.

interest (age, T stage, and MCDI).(Fig. 5B). Based on these findings, a prognostic nomogram integrating MCDI score, age and T stage was constructed to provide individualized survival probability estimates (Fig. 5C). Patients were stratified into high- and low-score groups using the surv_cutpoint function. Kaplan-Meier analysis revealed a marked survival difference between these groups (log-rank P<0.001; Fig. 5D).

Collectively, these results establish MCDI as a reliable and independent prognostic indicator for COAD, linking m6A-regulated PCD gene expression with disease progression, patient survival and immune-related molecular alterations.

MCDI predicts immunotherapy response and characterizes the immune microenvironment in COAD. Given the enrichment of immune-related pathways in the MCDI-associated gene signature, its immunologic and therapeutic relevance were systematically evaluated. First, the relationship between the MCDI score and the expression of key immunomodulators in the TCGA-COAD cohort was assessed. Spearman correlation analysis revealed that MCDI score was significantly associated with a broad array of molecules, including PDCD1LG2 (PD-L2), CD276 (B7-H3), TNFRSF4 (OX40), IL12A, IL1B, VEGFA, TGFB1 and ADORA2A, indicating potential immunoregulatory significance of the MCDI signature (Fig. 6A).

To further evaluate its predictive value for ICB therapy, the MCDI model was applied to independent immunotherapy cohorts (GSE67501, renal cell carcinoma; GSE78220, melanoma). In both datasets, patients with high MCDI scores exhibited markedly lower response rates to anti-PD-L1 treatment compared with those with low scores, suggesting that MCDI-low tumors may be more responsive to ICB therapy (Fig. 6B and C).

To elucidate the cellular composition of the tumor immune microenvironment, the CIBERSORT tool was applied to estimate the relative abundances of 22 immune cell types in TCGA-COAD samples. This analysis revealed significant differences in immune cell composition between the MCDI-defined risk groups. Compared with the low-risk group, the high-risk group exhibited significantly increased infiltration of M0 macrophages, plasma cells, $CD4^+$ memory resting T cells and regulatory T cells (Tregs), whereas monocytes were significantly decreased. Other immune cell types did not show significant differences between the two groups (Fig. 6D and E).

Consistent with these findings, TIDE analysis was performed to quantitatively assess immune evasion potential. The MCDI-high group showed significantly higher TIDE scores, indicating a microenvironment with enhanced immune evasion and impaired antitumor immune activity (Fig. 7A-C). The relationship between MCDI risk score and two key genomic biomarkers for immunotherapy (TMB and MSI status) were further examined. No significant association or correlation was observed between the MCDI and either TMB

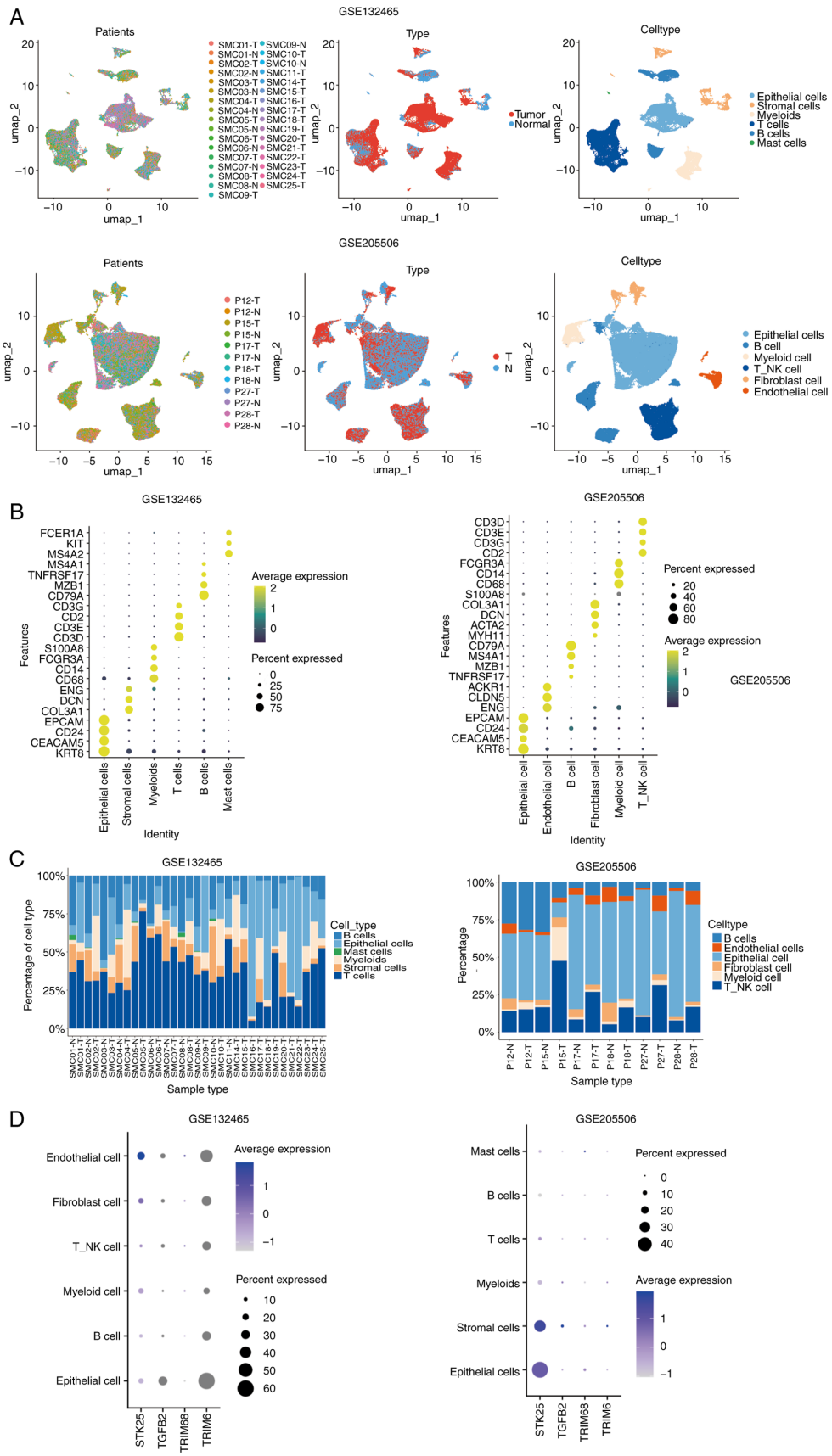

Figure 8. Single-cell transcriptomic atlas of COAD tissues reveals cell-type-specific expression patterns. (A) UMAP visualization of cells from COAD tissues, annotated by patient origin, tissue type and the six major identified cell types. (B) Bubble plots showing the expression of 23 canonical marker genes across the six cell types. Bubble size indicates the proportion of cells expressing each marker and color intensity reflects the average expression level. (C) Bar charts illustrating the relative proportions of the different cell types within COAD tissues. (D) Dot plots depicting the expression patterns of STK25, TGFB2, TRIM68 and TRIM6 across the six major cell types. Dot size represents the percentage of cells expressing each gene and color intensity indicates the average expression level. COAD, colon adenocarcinoma; STK25, serine/threonine kinase 25; TGFB2, transforming growth factor β2; TRIM68, tripartite motif containing 68; TRIM6, tripartite motif containing 6; T_NK, natural killer T cells.

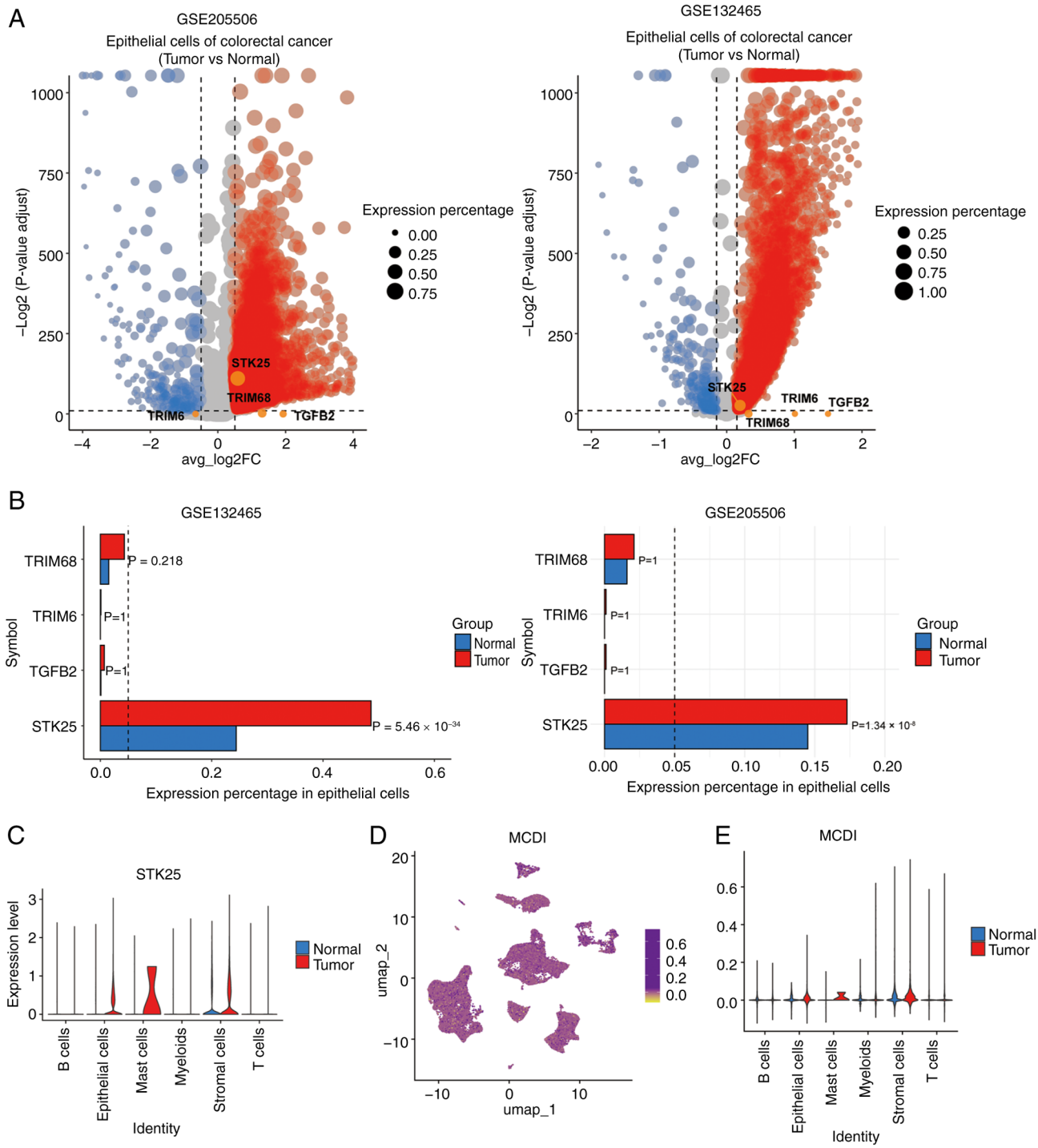

Figure 9. Tumor epithelial cell-specific enrichment of STK25 and MCDI score distribution at single-cell resolution. (A) Volcano plots of differentially expressed genes between tumor-derived and normal epithelial cells. Red and blue dots indicate genes significantly upregulated and downregulated in tumor epithelial cells, respectively. (B) Bar plots summarizing the mean expression proportion, fold change and adjusted P-values for TRIM68, TRIM6, TGFB2 and STK25 in tumor versus normal epithelial cells. (C) Violin plot illustrating STK25 expression levels across different cell types. (D) UMAP plot showing the single-cell-level distribution of the MCDI score. (E) Violin plot depicting the distribution of MCDI scores across different cell types. MCDI, m6A-PCD integrated signature; PCD, programmed cell death; STK25, serine/threonine kinase 25; TRIM68, tripartite motif containing 68; TRIM6, tripartite motif containing 6; TGFB2, transforming growth factor β2.

or MSI in the TCGA-COAD cohort (Fig. 7D-F), suggesting that the prognostic and immunological features captured by the MCDI may operate independently of these established biomarkers.

Together, these results indicate that MCDI may not only predict patient prognosis but also reflect distinct immunological states and potential responsiveness to immune checkpoint inhibitors in COAD.

Single-cell profiling identifies STK25 as a tumor-enriched MCDI core gene in COAD. To identify key genes driving MCDI-associated phenotypes, multivariate Cox regression

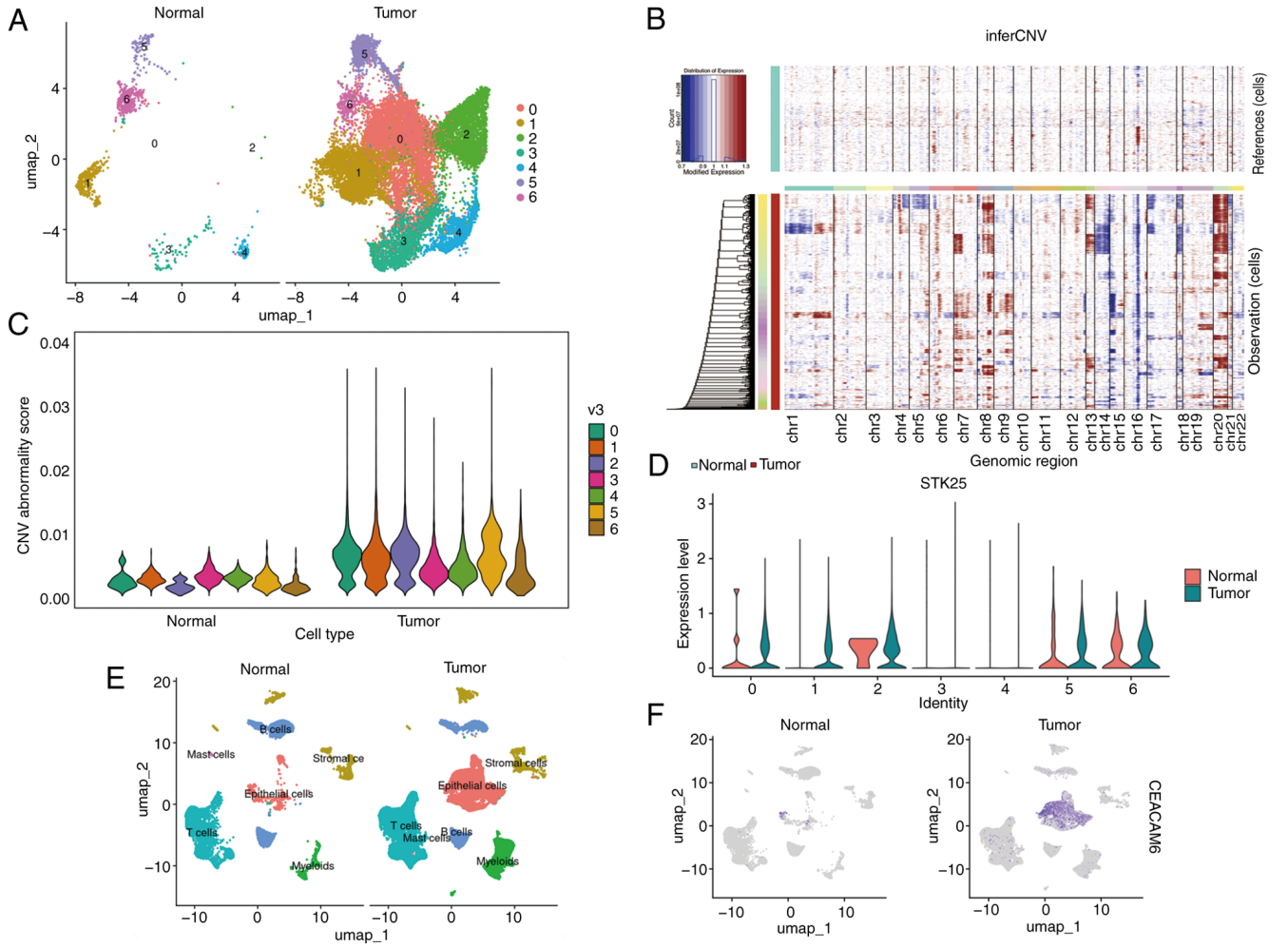

Figure 10. STK25 is specifically enriched in CNV-defined malignant epithelial subpopulations. (A) UMAP plot of epithelial cells from normal and tumor colon adenocarcinoma tissues, colored by cluster identity (clusters 0-6). (B) inferCNV heatmap depicting chromosomal CNVs across epithelial cell clusters. The upper panel shows reference cells, and the lower panel shows observation cells. Rows represent individual cell hierarchically clustered by similarity and columns represent genomic regions ordered by chromosomes (chr1-chr22). Red indicates copy number gains and blue indicates copy number losses. (C) Violin plots comparing CNV abnormality scores between normal and tumor epithelial cells across clusters 0-6. For each cluster, normal cells (left) and tumor cells (right) are shown, with tumor cells generally exhibiting higher CNV scores. (D) Violin plots showing STK25 expression levels across epithelial cell clusters, highlighting differential expression patterns among subpopulations. (E) UMAP visualization of major cell types in normal and tumor tissues. (F) UMAP plots illustrating the distribution of CEACAM6 expression. STK25, serine/threonine kinase 25; CNV, copy number variation; CEACAM6, carcinoembryonic antigen-related cell adhesion molecule 6.

analysis was first performed on the 21-gene signature. This analysis highlighted 5 genes (MIR210, STK25, TGFB2, TRIM6 and TRIM68) as independent prognostic factors for COAD (Fig. 2G). To examine the cellular context of these genes, scRNA-seq data from colon cancer tissues (GSE132465) were analyzed. After stringent QC and batch-effect correction via RPCA integration, six major cell populations were identified (epithelial, stromal, myeloid and T, B and mast cells) and annotated based on canonical marker gene expression (Fig. 8A-C). To systematically evaluate core prognostic gene expression across cell types, a dot plot was generated for STK25, TGFB2, TRIM68 and TRIM6 (Fig. 8D), revealing distinct cell-type-specific expression patterns.

STK25 was markedly upregulated in tumor epithelial cells compared with epithelial cells derived from adjacent normal tissues, highlighting its elevated expression in the malignant epithelial compartment, whereas TRIM6, TRIM68 and TGFB2 were expressed at low or undetectable levels in this cell type (Fig. 9A and B). Notably, STK25 expression was also enriched in mast cells within tumor tissues, suggesting potential roles in both epithelial and immune compartments (Fig. 9C). Consistent with this pattern, the MCDI score projected at the single-cell level was predominantly enriched in epithelial and mast cell populations from tumor tissues. Notably, enrichment was also observed in stromal cells, paralleling the STK25 distribution and further supporting its contribution to the high-risk phenotype (Fig. 9D and E).

To confirm the reproducibility of the single-cell observations, particularly the tumor-specific enrichment of STK25 in epithelial cells, an independent colon cancer scRNA-seq dataset (GSE205506) was analyzed. Consistently, STK25 was markedly upregulated in tumor-derived epithelial cells, whereas TRIM6, TRIM68 and TGFB2 remained minimally expressed across cell types (Fig. 8A-D).

To further validate the epithelial origin of STK25 enrichment and its association with malignancy, re-clustering of

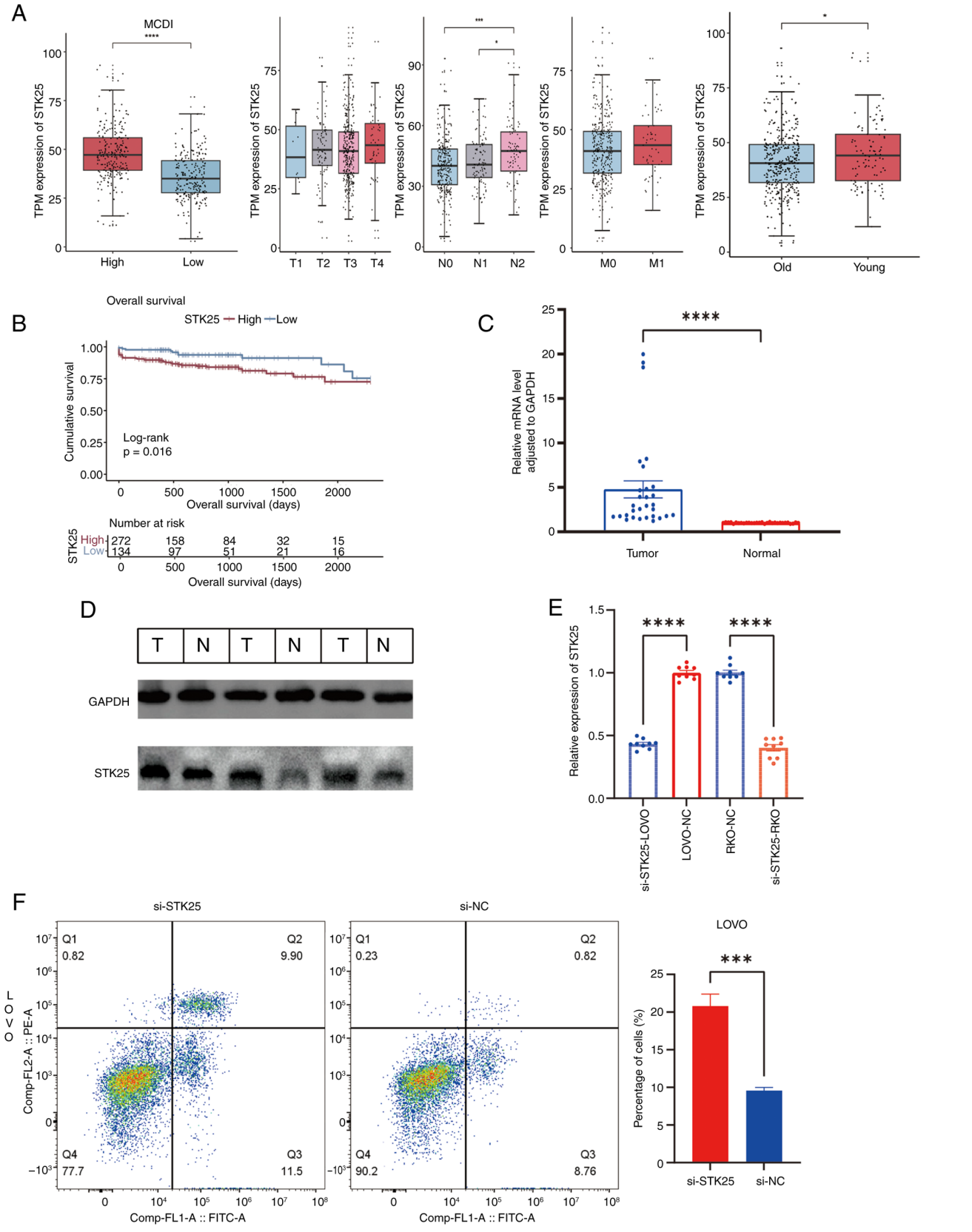

Figure 11. Clinical significance, expression validation and oncogenic function of STK25. (A) Box plots depicting the association between STK25 expression and clinical parameters, including MCDI score, T stage, N stage, M stage and patient age (old, >55 years; young, ≤55 years). Comparisons were performed using the Wilcoxon rank-sum test. (B) Kaplan-Meier overall survival curves comparing patients with high versus low STK25 expression, stratified by the median expression level, in the The Cancer Genome Atlas-colon adenocarcinoma cohort. (C) RT-qPCR validation of relative STK25 mRNA expression in 10 paired colon cancer and adjacent normal tissue samples. (D) Western blot validation of STK25 protein expression in three representative paired colon cancer and adjacent normal tissues, with GAPDH as the loading control. (E) Validation of STK25 knockdown efficiency in RKO and LOVO cells using siRNA, measured by RT-qPCR. (F) Apoptosis analysis in LOVO cells after STK25 knockdown, assessed by Annexin V-FITC/PI flow cytometry. *P<0.05, ***P<0.001, ****P<0.0001. RT-qPCR, reverse transcription-quantitative PCR; MCDI, m6A-PCD integrated signature; PCD, programmed cell death; STK25, serine/threonine kinase 25; siRNA, small interfering RNA; NC, negative control.

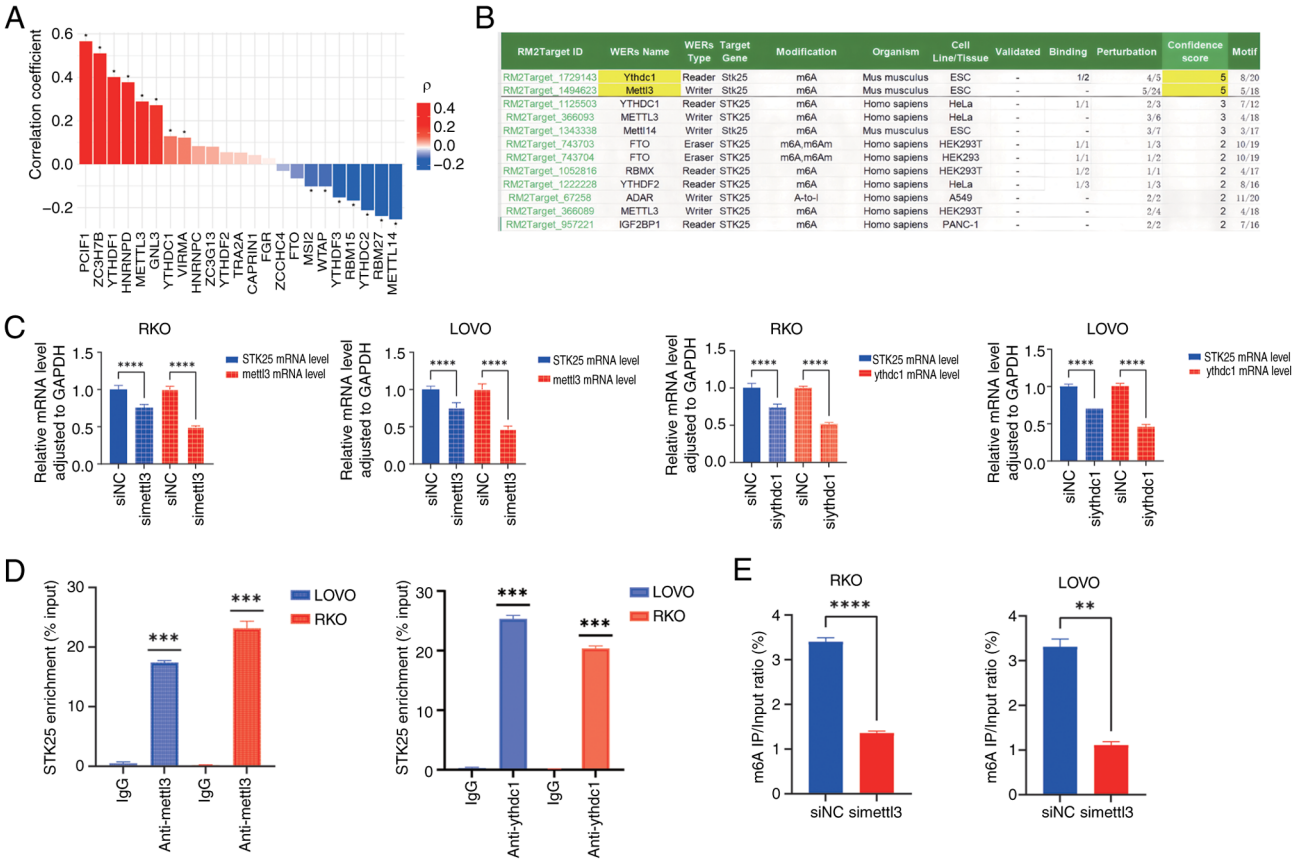

Figure 12. METTL3/YTHDC1 regulates STK25 mRNA stability via m6A modification. (A) Bar plot showing Spearman correlation coefficients between STK25 and 23 m6A regulators. Red bars indicate positive correlations; blue bars indicate negative correlations and color intensity reflects correlation strength. (B) Credibility scores of m6A regulators predicted to target STK25, as obtained from the RM2Target database. (C) Reverse transcription-qPCR analysis of STK25 mRNA levels in RKO and LOVO cells following knockdown of METTL3 or YTHDC1. (D) RIP assay using METTL3 and YTHDC1 antibodies, showing enrichment of STK25 mRNA compared with IgG control. (E) MeRIP-qPCR analysis of m6A modification on STK25 mRNA in control and METTL3-knockdown cells, demonstrating decreased m6A enrichment upon METTL3 knockdown. *P<0.05, **P<0.01, ***P<0.001, ****P<0.0001. qPCR, quantitative PCR; RIP, RNA immunoprecipitation; MeRIP, methylated RNA immunoprecipitation; METTL3, methyltransferase-like 3; YTHDC1, YTH domain containing 1; STK25, serine/threonine kinase 25; si, small interfering RNA; NC, negative control.

epithelial cells from the integrated GSE132465 dataset was performed, identifying 7 distinct subclusters (Cluster 0-6) (Fig. 10A). Subsequent inferCNV analysis, visualized via a heatmap of chromosomal CNVs (Fig. 10B) and violin plots comparing CNV aberration scores (Fig. 10C), revealed that Clusters 0, 1, 2 and 5 exhibited significantly elevated CNV scores relative to the normal control group, indicating that these subclusters represent malignant epithelial cells. Notably, within the GSE132465 cohort, high STK25 expression (Fig. 10D), along with the established malignant epithelial marker CEACAM6 (Fig. 10E and F), was predominantly concentrated in these CNV-defined malignant subclusters (Clusters 0, 1, 2 and 5) from tumor samples, providing cross-validation and confirming tumor-specific enrichment.

Collectively, these results consistently highlighted STK25 as a tumor-enriched, prognostically relevant MCDI core gene, supporting its selection for further functional investigation.

STK25 expression is associated with tumor progression and apoptosis suppression in COAD. The expression profile and clinical significance of STK25 in COAD was next evaluated. The Wilcoxon rank-sum test revealed that STK25 expression was significantly higher in patients with elevated MCDI scores. STK25 expression did not show significant differences across tumor stages (T stage) or distant metastasis status (M stage). However, higher expression levels were observed in patients with lymph node metastasis, particularly in the N2 group (Fig. 11A). Although STK25 expression showed a modest upward trend in distant metastasis (M stage), this did not reach statistical significance. Notably, younger patients exhibited slightly higher STK25 expression than older patients (Fig. 11A). Patients were divided into high- and low-expression groups based on the median STK25 level. Kaplan-Meier survival analysis demonstrated that patients with high STK25 expression had a significantly poorer OS compared with those with low expression (Fig. 11B), indicating that elevated STK25 may be associated with aggressive tumor behavior and an unfavorable prognosis.

To validate the differential expression results, qPCR and western blot analyses were performed on paired tumor and adjacent normal tissues, which consistently showed markedly higher STK25 expression in tumor tissues (Fig. 11C and D). Functional assays further explored the biological role of STK25; STK25 knockdown in LOVO cells, confirmed by qPCR (Fig. 11E), significantly increased apoptosis, as measured by flow cytometry (Fig. 11F).

Collectively, these findings indicated that STK25 may promote colon cancer progression, at least in part by suppressing apoptosis, supporting its role as a potential oncogenic driver and therapeutic target.

METTL3/YTHDC1-mediated m6A modification stabilizes STK25 mRNA in COAD. The upstream mechanisms driving STK25 upregulation were next investigated, focusing on potential regulation via m6A-dependent post-transcriptional modification. Spearman correlation analysis between STK25 and 23 known m6A regulators in the TCGA-COAD cohort revealed a distinct pattern: STK25 expression was positively correlated with PCIF1, ZC3H7B, YTHDF1, HNRNPD, METTL3, GNL3 and YTHDC1, while negatively correlated with METTL14, RBM27, YTHDC2, RBM15, YTHDF3, WTAP and MSI2 (Fig. 12A).

To identify the most credible upstream regulators, the RM2Target database was queried using STK25 as the target gene. METTL3 and YTHDC1 emerged as the highest-confidence regulators predicted to target STK25 (Fig. 12B), as they showed the highest confidence scores in RM2Target and were supported by binding and perturbation evidence. Both regulators also exhibited positive associations with STK25 expression, suggesting a potential regulatory mechanism involving m6A installation by METTL3 and subsequent recognition by YTHDC1. Functionally, METTL3, as an m6A 'writer', deposits m6A markers on RNA, while YTHDC1, a nuclear m6A 'reader', binds methylated transcripts to enhance stability. Consistent with this mechanism, knocking down METTL3 or YTHDC1 expression in RKO and LOVO cells reduced STK25 mRNA levels (Fig. 12C).

To determine if this regulation is direct, RIP assays were performed using antibodies against METTL3 and YTHDC1. RIP-qPCR demonstrated significant enrichment of STK25 transcripts in both METTL3 and YTHDC1 IPs compared with IgG controls (Fig. 12D), confirming direct physical interaction with STK25 mRNA. Finally, MeRIP-qPCR was conducted to verify METTL3-mediated m6A modification of STK25. Following METTL3 knockdown, m6A enrichment on STK25 mRNA was significantly reduced (Fig. 12E).

Collectively, these results demonstrated that METTL3-catalyzed m6A methylation and YTHDC1 recognition cooperatively enhanced STK25 mRNA stability, establishing an m6A-YTHDC1-STK25 axis that promotes COAD progression, with METTL3 knockdown effectively suppressing STK25 expression.

Discussion

In the present study, an integrated MCDI for COAD capable of stratifying patient survival and predicting response to PD-1/PD-L1 immunotherapy was developed. Within this signature, STK25 emerged as a previously unrecognized, tumor-enriched driver that may promote tumor progression by suppressing apoptosis. Mechanistically, a novel m6A-dependent METTL3-YTHDC1-STK25 axis was uncovered, which may stabilize STK25 mRNA and a possible direct link between m6A regulation and PCD in COAD was established.

Despite continued reliance on clinicopathological indicators, prognostic performance in COAD remains inconsistent across genetically heterogeneous patients (12,28-31). This inconsistency is further compounded by prior studies, which largely modeled either m6A regulation or individual PCD pathways in isolation (32-41). By contrast, the present study integrated these layers into a single transcriptomic signature, the MCDI, providing independent risk stratification of the TCGA-COAD cohort, which was externally validated using GSE39582, GSE33113 and GSE38832 (31,42). This integrative strategy captured complementary biological information: m6A functions upstream at the post-transcriptional level, whereas PCD represents downstream execution programs that determine cell fate (43-45). Therefore, joint modeling provides a more comprehensive readout of tumor state than either layer alone, enhancing discriminative power and robustness, as confirmed by the internal TCGA and external cohort validations. By coupling the global regulatory influence of m6A with the key effector pathways of PCD, the model captures regulatory mechanisms that are shared across diverse molecular backgrounds. This integrative design enables the model to maintain predictive performance across heterogeneous tumor subtypes, consistent with its independent prognostic value across clinical strata observed in the present study (4,6,46-48).

Compared with previous models focusing on a single dimension either m6A regulation alone or individual PCD pathways (49,50), the integrated approach of the present study demonstrates improved predictive performance. In the external validation cohorts (GSE39582 and GSE38832), the MCDI achieved AUC values of 0.783-0.805 for 1-year and 0.699-0.711 for 3-year OS, outperforming recently reported single-mechanism prognostic signatures, including those by Ma *et al* (51) (1-year AUC: 0.66; 3-year AUC: 0.67), Qiao *et al* (52) (AUC range: 0.516-0.607) and Zhu *et al* (53) (1-year AUC: 0.67; 3-year AUC: 0.67).

Beyond this performance advantage, the MCDI framework not only offers improved risk stratification but also enhances mechanistic insight and clinical relevance. Conventional single-dimensional models are often limited to identifying correlations, whereas the integrated analysis of the present study led to the discovery of a novel METTL3-YTHDC1-STK25 regulatory axis. Experimental validation demonstrated that this axis may stabilize STK25 mRNA in an m6A-dependent manner, thereby suppressing cancer cell apoptosis. This finding directly links upstream epitranscriptomic regulation with downstream execution of cell death, providing a mechanistic explanation for the prognostic power of the MCDI, an insight rarely achievable with single-pathway models.

Furthermore, since PCD modalities shape antitumor immunity (54,55) and m6A broadly regulates transcripts involved in both immune function and PCD (56), an integrated signature such as the MCDI naturally connects to immune checkpoint activity and can predict PD-1/PD-L1 responsiveness. Notably, in the present study, no significant association was observed between the MCDI score and the TMB or MSI status. This may reflect two possibilities: First, that the direct clinical utility of MCDI for predicting response to current immune checkpoint inhibitors requires further validation; second, more plausibly, that the model captures a distinct biological mechanism operating independently of the conventional TMB/MSI framework. High MCDI scores were associated with the enrichment of M0 macrophages and

Tregs, a reduction in cytotoxic immune cells and an increased immune evasion potential, as indicated by the TIDE scores, delineating a unique immunosuppressive microenvironment. These observations suggest that tumor-intrinsic properties shaped by the m6A-PCD network may represent an alternative pathway of immune evasion. Therefore, the strength of the MCDI lies in uncovering biological mechanisms that function independently of TMB/MSI, rather than serving as a direct substitute for existing predictive biomarkers. This integrated framework enhances mechanistic interpretability by linking pathway imbalances to traceable epigenetic regulation.

The core prognostic gene STK25 within the MCDI signature exemplifies the mechanistic link between m6A regulation and PCD while providing novel insights into its clinical relevance. Previous studies have associated STK25 with tumor progression through metabolic and signaling pathways promoting lipid metabolic reprogramming and proliferation via striatin-AMP-activated protein kinase-acetyl-CoA carboxylase 1 in hepatocellular carcinoma (57) and facilitating COAD growth by restraining autophagy through JAK2-STAT3 (58). While these reports established biological plausibility, they did not position STK25 within a clinically validated, multi-gene framework or define its spatial distribution in human tumors. The present study extends these findings by embedding STK25 within an integrated m6A-PCD prognostic context. Within the MCDI, STK25 functions as an independent risk factor in COAD: higher expression was associated with a poorer OS, advanced T/N stage and tumor-enriched expression localized primarily to epithelial cells, with additional expression in mast-cell compartments, at single-cell resolution. Thus, beyond pathway-centric observations, STK25 is now linked to a risk model that generalizes across clinical strata and may be related to immunotherapy response, enhancing its clinical relevance for patient stratification and mechanistic hypothesis generation.

Mechanistically, the present study delineated a previously unreported m6A-dependent METTL3-YTHDC1-STK25 axis in COAD. METTL3 (m6A writer) and YTHDC1 (nuclear reader) may cooperate to stabilize STK25 mRNA and perturbation of either component may reduce STK25 levels and increase apoptosis. These findings suggest that STK25 functions as a mechanistically relevant effector rather than merely a correlative marker. This may explain its sustained upregulation in tumors and its integration with the cell death-related biology captured by the MCDI model. Moreover, the results highlight potential therapeutic intervention points both upstream, through modulation of m6A writer/reader activity, and downstream, through targeting STK25-mediated anti-apoptotic effects. Consistent with the findings of the present study, prior studies have shown that METTL3-mediated m6A modification promotes oncogenic signaling in colon cancer through multiple downstream targets, including JAK1-STAT3 activation via YTHDF1-mediated translation (59) and m6A-dependent silencing of suppressor of cytokine signaling 2 mRNA (60). These convergent observations underscore METTL3 as a central m6A writer orchestrating key oncogenic pathways in COAD, with the METTL3-YTHDC1-STK25 axis adding a distinct apoptosis-regulatory dimension.

Although the MCDI prognostic model developed in the present study demonstrated significant value for predicting colon cancer outcomes, several limitations should be acknowledged: i) Cohort size and validation depth: The model was primarily constructed and validated using publicly available cohorts such as TCGA, which have relatively limited sample sizes. Future studies should incorporate multi-center, large-sample prospective cohorts to further assess the generalizability and stability of the model, particularly across diverse ethnicities, clinical stages and treatment backgrounds. ii) Need for improved predictive performance: While the model demonstrated promising discriminative ability in survival prediction, further optimization is possible. Integrating additional data modalities, such as methylation and proteomics, as well as radiomics and clinicopathological features, may improve risk stratification and enhance predictive performance. iii) Mechanistic validation of the METTL3/YTHDC1-STK25 axis: Although the findings of the present study robustly supported this regulatory axis via correlation analysis, knockdown experiments, RIP and MeRIP-qPCR assays, further mechanistic studies such as direct measurement of STK25 mRNA stability (including actinomycin D chase assays) and functional rescue experiments are warranted to fully delineate the post-transcriptional regulatory mechanism. While these limitations may affect the generalizability of the findings of the present study, they also provide clear directions for future research. Subsequent work should focus on expanding the validation cohorts, optimizing the model architecture and deeper mechanistic exploration to facilitate clinical translation of the MCDI model.

In conclusion, the present study described a robust, integrated MCDI that predicts survival and PD-1/PD-L1 immunotherapy response in COAD. Additionally, a previously unreported METTL3-YTHDC1-STK25 axis that links epitranscriptomic regulation to apoptosis resistance was identified. This framework combined prognostic stratification with mechanistic insight, supporting clinical translation: MCDI may enable risk prediction and patient stratification, while the STK25-m6A axis may provide actionable therapeutic targets and potential biomarkers. Future research should focus on validation of the MCDI framework in dedicated COAD immunotherapy cohorts to clarify its clinical predictive value and to explore combination strategies targeting the immunosuppressive microenvironment it delineates, potentially through core effectors such as STK25.

Acknowledgements

Not applicable.

Funding

This research was supported by the Operating Funds for Fujian Clinical Research Center for Digestive System Tumors and Upper Gastrointestinal Diseases (grant no. 2022YGPT004), the National Key Clinical Specialty Construction Projects of Fujian Province, China (grant no. 2023-1594) and the Construction Project of Fujian Province Minimally Invasive Medical Center (grant no. 2021-76).

Availability of data and materials

The data generated in the present study may be requested from the corresponding author.

Authors' contributions

HZY and FLC conducted the experiments, performed bioinformatics analyses, interpreted the data and drafted the manuscript. ZHC and ZXL were responsible for sample collection. XYH, THL and FLC conceived and designed the study. FLC supervised the project and provided critical revisions. All authors read and approved the final manuscript. HZY and FLC confirm the authenticity of all the raw data.

Ethics approval and consent to participate

This study was approved by the Ethics Committee of Fujian Medical University Union Hospital (approval no. 2025KY307). All participants provided written informed consent after being fully informed about the study procedures.

Patient consent for publication

Not applicable.

Competing interests

The authors declare that they have no competing interests.

References

1. Bray F, Laversanne M, Sung H, Ferlay J, Siegel RL, Soerjomataram I and Jemal A: Global cancer statistics 2022: GLOBOCAN estimates of incidence and mortality worldwide for 36 cancers in 185 countries. CA Cancer J Clin 74: 229-263, 2024.
2. Ciardiello D, Guerrera LP, Maiorano BA, Parente P, Latiano TP, Di Maio M, Ciardiello F, Troiani T, Martinelli E and Maiello E: Immunotherapy in advanced anal cancer: Is the beginning of a new era? Cancer Treat Rev 105: 102373, 2022.
3. Miller KD, Nogueira L, Devasia T, Mariotto AB, Yabroff KR, Jemal A, Kramer J and Siegel RL: Cancer treatment and survivorship statistics, 2022. CA Cancer J Clin 72: 409-436, 2022.
4. Wu Q, Fu X, He X, Liu J, Li Y and Ou C: Experimental prognostic model integrating N6-methyladenosine-related programmed cell death genes in colorectal cancer. Science 27: 108720, 2024.
5. Chen J, Ye M, Bai J, Hu C, Lu F, Gu D, Yu P and Tang Q: Novel insights into the interplay between m6A modification and programmed cell death in cancer. Int J Biol Sci 19: 1748-1763, 2023.
6. Liu L, Li H, Hu D, Wang Y, Shao W, Zhong J, Yang S, Liu J and Zhang J: Insights into N6-methyladenosine and programmed cell death in cancer. Mol Cancer 21: 32, 2022.
7. Boulias K and Greer EL: Biological roles of adenine methylation in RNA. Nat Rev Genet 24: 143-160, 2023.
8. Jiang X, Liu B, Nie Z, Duan L, Xiong Q, Jin Z, Yang C and Chen Y: The role of m6A modification in the biological functions and diseases. Signal Transduct Target Ther 6: 74, 2021.
9. Liu J, Harada BT and He C: Regulation of gene expression by N6-methyladenosine in cancer. Trends Cell Biol 29: 487-499, 2019.
10. Wei S, Han C, Mo S, Huang H and Luo X: Advancements in programmed cell death research in antitumor therapy: A comprehensive overview. Apoptosis 30: 401-421, 2025.
11. Park W, Wei S, Kim BS, Kim B, Bae SJ, Chae YC, Ryu D and Ha KT: Diversity and complexity of cell death: A historical review. Exp Mol Med 55: 1573-1594, 2023.
12. Sun ZQ, Ma S, Zhou QB, Yang SX, Chang Y, Zeng XY, Ren WG, Han FH, Xie X, Zeng FY, *et al*: Prognostic value of lymph node metastasis in patients with T1-stage colorectal cancer from multiple centers in China. World J Gastroenterol 23: 8582-8590, 2017.
13. Qu Y, Gao N, Zhang S, Gao L, He B, Wang C, Gong C, Shi Q, Li Z, Yang S and Xiao Y: Role of N6-methyladenosine RNA modification in cancer. Med Comm 5: e715, 2024, 2020.
14. Chen X, Xu M, Xu X, Zeng K, Liu X, Pan B, Li C, Sun L, Qin J, Xu T, *et al*: METTL14-mediated N6-methyladenosine modification of SOX4 mRNA inhibits tumor metastasis in colorectal cancer. Mol Cancer 19: 106, 2020.
15. Liu Y, Guo F, Guo W, Wang Y, Song W and Fu T: Ferroptosis-related genes are potential prognostic molecular markers for patients with colorectal cancer. Clin Exp Med 21: 467-477, 2021.
16. Wu LS, Liu Y, Wang XW, Xu B, Lin YL, Song Y, Dong Y, Liu JL, Wang XJ, Liu S, *et al*: LPS enhances the chemosensitivity of oxaliplatin in HT29 cells via GSDMD-mediated pyroptosis. Cancer Manag Res 12: 10397-10409, 2020.
17. He Q, Li Z, Yin J, Li Y, Yin Y, Lei X and Zhu W: Prognostic significance of autophagy-relevant gene markers in colorectal cancer. Front Oncol 11: 566539, 2021.
18. Livak KJ and Schmittgen TD: Analysis of relative gene expression data using real-time quantitative PCR and the 2(-Delta Delta C(T)) method. Methods 25: 402-408, 2001.
19. Cao K, Zhu J, Lu M, Zhang J, Yang Y, Ling X, Zhang L, Qi C, Wei S, Zhang Y and Ma J: Analysis of multiple programmed cell death-related prognostic genes and functional validations of necroptosis-associated genes in oesophageal squamous cell carcinoma. EBioMedicine 99: 104920, 2024.
20. Wang R, Li Z and Shen J: Predicting prognosis and drug sensitivity in bladder cancer: An insight into pan-programmed cell death patterns regulated by M6A modifications. Sci Rep 14: 18321, 2024.
21. Marisa L, de Reyniès A, Duval A, Selves J, Gaub MP, Vescovo L, Etienne-Grimaldi MC, Schiappa R, Guenot D, Ayadi M, *et al*: Gene expression classification of colon cancer into molecular subtypes: Characterization, validation, and prognostic value. PLoS Med 10: e1001453, 2013.
22. Kemper K, Versloot M, Cameron K, Colak S, de Sousa e Melo F, de Jong JH, Bleackley J, Vermeulen L, Versteeg R, Koster J and Medema JP: Mutations in the Ras-Raf Axis underlie the prognostic value of CD133 in colorectal cancer. Clin Cancer Res 18: 3132-3141, 2012.
23. Tripathi MK, Deane NG, Zhu J, An H, Mima S, Wang X, Padmanabhan S, Shi Z, Prodduturi N, Ciombor KK, *et al*: Nuclear factor of activated T-cell activity is associated with metastatic capacity in colon cancer. Cancer Res 74: 6947-6957, 2014.
24. Ascierto ML, McMiller TL, Berger AE, Danilova L, Anders RA, Netto GJ, Xu H, Pritchard TS, Fan J, Cheadle C, *et al*: The intratumoral balance between metabolic and immunologic gene expression is associated with anti-PD-1 response in patients with renal cell carcinoma. Cancer Immunol Res 4: 726-733, 2016.
25. Hugo W, Zaretsky JM, Sun L, Song C, Moreno BH, Hu-Lieskovan S, Berent-Maoz B, Pang J, Chmielowski B, Cherry G, *et al*: Genomic and transcriptomic features of response to anti-PD-1 therapy in metastatic melanoma. Cell 165: 35-44, 2016.
26. Lee HO, Hong Y, Etlioglu HE, Cho YB, Pomella V, Van den Bosch B, Vanhecke J, Verbandt S, Hong H, Min JW, *et al*: Lineage-dependent gene expression programs influence the immune landscape of colorectal cancer. Nat Genet 52: 594-603, 2020.
27. Li J, Wu C, Hu H, Qin G, Wu X, Bai F, Zhang J, Cai Y, Huang Y, Wang C, *et al*: Remodeling of the immune and stromal cell compartment by PD-1 blockade in mismatch repair-deficient colorectal cancer. Cancer Cell 41: 1152-1169.e7, 2023.
28. Liao CK, Yu YL, Lin YC, Hsu YJ, Chern YJ, Chiang JM and You JF: Prognostic value of the C-reactive protein to albumin ratio in colorectal cancer: An updated systematic review and meta-analysis. World J Surg Oncol 19: 139, 2021.
29. Huang X, Liu H, Liao X, Xiao Z, Huang Z and Li G: Prognostic factors for T1-2 colorectal cancer after radical resection: Lymph node distribution is a valuable predictor of its survival. Asian J Surg 44: 241-246, 2021.
30. Pathak PS, Chan G, Deming DA and Chee CE: State-of-the-art management of colorectal cancer: Treatment advances and innovation. Am Soc Clin Oncol Educ Book 44: e438466, 2024.
31. Zygulska AL and Pierzchalski P: Novel diagnostic biomarkers in colorectal cancer. Int J Mol Sci 23: 852, 2022.
32. Zhang L, Mao Z, Yin K and Wang S: Review of METTL3 in colorectal cancer: From mechanisms to the therapeutic potential. Int J Biol Macromol 277: 134212, 2024.
33. Huang H, Weng H and Chen J: m6A modification in coding and non-coding RNAs: Roles and therapeutic implications in cancer. Cancer Cell 37: 270-288, 2020.
34. Ma M, Wang W, Li L, Wang X, Huang Q, Zhou C, Huang Y, Zhao G and Ye L: RBM15 facilities lung adenocarcinoma cell progression by regulating RASSF8 stability through N6 methyladenosine modification. Transl Oncol 46: 102018, 2024.
35. An Y and Duan H: The role of m6A RNA methylation in cancer metabolism. Mol Cancer 21: 14, 2022.

36. Huang YY, Bao TY, Huang XQ, Lan QW, Huang ZM, Chen YH, Hu ZD and Guo XG: Machine learning algorithm to construct cuproptosis- and immune-related prognosis prediction model for colon cancer. World J Gastrointest Oncol 15: 372-388, 2023.
37. Hu G, Yao H, Wei Z, Li L, Yu Z, Li J, Luo X and Guo Z: A bioinformatics approach to identify a disulfidptosis-related gene signature for prognostic implication in colon adenocarcinoma. Sci Rep 13: 12403, 2023.
38. Zhu J, Kong W and Xie Z: Expression and prognostic characteristics of ferroptosis-related genes in colon cancer. Int J Mol Sci 22: 5652, 2021.
39. Zhou J, Guo H, Liu L, Feng M, Yang X and Hao S: Pyroptosis patterns of colon cancer could aid to estimate prognosis, microenvironment and immunotherapy: Evidence from multi-omics analysis. Aging (Albany NY) 14: 7547-7567, 2022.
40. Zhu Q, Wu X, Ma L and Xue H: Apoptosis-associated gene expression profiling is one new prognosis risk predictor of human rectal cancer. Dis Markers 2022: 4596810, 2022.
41. Chen S, Wang Y, Wang B, Zhang L, Su Y, Xu M and Zhang M: A signature based on 11 autophagy genes for prognosis prediction of colorectal cancer. PLoS One 16: e0258741, 2021.
42. Tsimberidou AM, Fountzilas E, Bleris L and Kurzrock R: Transcriptomics and solid tumors: The next frontier in precision cancer medicine. Semin Cancer Biol 84: 50-59, 2022.
43. Gao L, Jiang Z, Han Y, Li Y and Yang X: Regulation of pyroptosis by ncRNA: A novel research direction. Front Cell Dev Biol 10: 840576, 2022.
44. Yang X, Mei C, Ma X, Du J, Wang J and Zan L: m6A methylases regulate myoblast proliferation, apoptosis and differentiation. Animals (Basel) 12: 773, 2022.
45. Zhu TY, Hong LL and Ling ZQ: Oncofetal protein IGF2BPs in human cancer: Functions, mechanisms and therapeutic potential. Biomark Res 11: 62, 2023.
46. Gao Y, Guo Q and Yu L: m6A modification of RNA in cervical cancer: Role and clinical perspectives. RNA Biol 21: 49-61, 2024.
47. Zhou Y, Cao P and Zhu Q: The regulatory role of m6A in cancer metastasis. Front Cell Dev Biol 13: 1539678, 2025.
48. Zhang X, Cao Y, Liu J, Wang W, Yan Q and Wang Z: Comprehensive analysis of m6A-related programmed cell death genes unveils a novel prognostic model for lung adenocarcinoma. J Cell Mol Med 29: e70255, 2025.
49. Wu Q, Chen L, Miao D, Jin Y and Zhu Z: Prognostic signature based on m6A-related lncRNAs to predict overall survival in pancreatic ductal adenocarcinoma. Sci Rep 12: 3079, 2022.
50. Yin L, Feng S, Sun Y, Jiang Y, Tang C and Sun D: Identification of a five m6A-relevant mRNAs signature and risk score for the prognostication of gastric cancer. J Gastrointest Oncol 13: 2234-2248, 2022
51. Ma B, Bao S and Li Y: Identification and validation of m6A-GPI signatures as a novel prognostic model for colorectal cancer. Front Oncol 13: 1145753, 2023.
52. Qiao S, Yang S, Hua H, Mao C, Li X, Cheng C, Guo H and Lu W: Identification of prognostic biomarkers in colorectal cancer through multi-omics profiling of programmed cell death pathways. J Gastrointest Oncol 16: 1503-1520, 2025.
53. Zhu H, Yang Y and Zhou Z: Construction and clinical application of a risk model based on N6-methyladenosine regulators for colorectal cancer. PeerJ 12: e18719, 2024.
54. Zhu ZZ, Zhang G and Liu J: Establishment of a novel prognostic prediction model for gastric cancer based on necroptosis-related genes. Pathol Oncol Res 28: 1610641, 2022.
55. Xia J, Zhuo W, Deng L, Yin S, Tang S, Yi L, Feng C, Zhong X, He Z, Sun B and Zhang C: BDNF is a prognostic biomarker involved in the immune infiltration of lung adenocarcinoma and associated with programmed cell death. Oncol Lett 29: 191, 2025.
56. Yan Y, Yin J, Ding Q, Lu Y, Gou S, Xu X and Li Y: M6A RNA modification: Focusing on non-small cell lung cancer progression, therapeutic strategies and challenges. Front Oncol 15: 1622359. 2025.
57. Zhang Y, Xu J, Qiu Z, Guan Y, Zhang X, Zhang X, Chai D, Chen C, Hu Q and Wang W: STK25 enhances hepatocellular carcinoma progression through the STRN/AMPK/ACC1 pathway. Cancer Cell Int 22: 4, 2022.
58. Chen J, Gao P, Peng L, Liu T, Wu F, Xu K, Chen L, Tan F, Xing P, Wang Z, *et al*: Downregulation of STK25 promotes autophagy via the janus kinase 2/signal transducer and activator of transcription 3 pathway in colorectal cancer. Mol Carcinog 61: 572-586, 2022.
59. Sun Y, Gong W and Zhang S: METTL3 promotes colorectal cancer progression through activating JAK1/STAT3 signaling pathway. Cell Death Dis 14: 765, 2023.
60. Xu J, Chen Q, Tian K, Liang R, Chen T, Gong A, Mathy N.W, Yu T and Chen X: m6A methyltransferase METTL3 maintains colon cancer tumorigenicity by suppressing SOCS2 to promote cell proliferation. Oncol Rep 44: 973-986, 2020.